

Article (refereed) - postprint

Ascott, M.J.; Goody, D.C.; Lapworth, D.J.; Davidson, P.; Bowes, M.J.; Jarvie, H.P.; Surridge, B.W.J. 2018. **Phosphorus fluxes to the environment from mains water leakage: seasonality and future scenarios.** *Science of the Total Environment*, 636. 1321-1332.
<https://doi.org/10.1016/j.scitotenv.2018.04.226>

© 2018 BGS/UKRI. Published by Elsevier B.V.

This manuscript version is made available under the CC-BY-NC-ND 4.0 license <http://creativecommons.org/licenses/by-nc-nd/4.0/>



This version available <http://nora.nerc.ac.uk/id/eprint/519975/>

NERC has developed NORA to enable users to access research outputs wholly or partially funded by NERC. Copyright and other rights for material on this site are retained by the rights owners. Users should read the terms and conditions of use of this material at <http://nora.nerc.ac.uk/policies.html#access>

NOTICE: this is the author's version of a work that was accepted for publication in *Science of the Total Environment*. Changes resulting from the publishing process, such as peer review, editing, corrections, structural formatting, and other quality control mechanisms may not be reflected in this document. Changes may have been made to this work since it was submitted for publication. A definitive version was subsequently published in *Science of the Total Environment*, 636. 1321-1332.
<https://doi.org/10.1016/j.scitotenv.2018.04.226>

www.elsevier.com/

Contact CEH NORA team at
noraceh@ceh.ac.uk

1 **Global assessment of the effect of climate change on ammonia**
2 **emissions from seabirds.**

3 S. N. Riddick^{1,2,*}, U. Dragosits¹, T. D. Blackall², S. J. Tomlinson¹, F. Daunt¹, S.
4 Wanless¹, S. Hallsworth¹, C. F. Braban¹, Y. S. Tang¹ and M. A. Sutton¹

5 ¹ Centre for Ecology & Hydrology Edinburgh, Bush Estate, Midlothian, UK

6 ² King's College London, Strand, London, UK

7 * now at Princeton University, Princeton, NJ, USA

8 **Key Words:** Seabirds; Global NH₃ emission; Process-based modelling, Climate
9 change

10 **Abstract**

11 Seabird colonies alter the biogeochemistry of nearby ecosystems, while the
12 associated emissions of ammonia (NH₃) may cause acidification and eutrophication
13 of finely balanced biomes. To examine the possible effects of future climate change
14 on the magnitude and distribution of seabird NH₃ emissions globally, a global
15 seabird database was used as input to the GUANO model, a dynamic mass-flow
16 process-based model that simulates NH₃ losses from seabird colonies at an hourly
17 resolution in relation to environmental conditions. Ammonia emissions calculated
18 by the GUANO model were in close agreement with measured NH₃ emissions
19 across a wide range of climates. For the year 2010, the total global seabird NH₃
20 emission is estimated at 82 [37 - 127] Gg year⁻¹. This is less than previously
21 estimated using a simple temperature-dependent empirical model, mainly due to
22 inclusion of nitrogen wash-off from colonies during precipitation events in the
23 GUANO model. High precipitation, especially between 40° and 60° S, results in
24 total emissions for the penguin species that are 82% smaller than previously
25 estimated, while for species found in dry tropical areas, emissions are 83 - 133%
26 larger. Application of temperature anomalies for several IPCC scenarios for 2099
27 in the GUANO model indicated a predicted net increase in global seabird NH₃
28 emissions of 27% (B1 scenario) and 39% (A2 scenario), compared with the 2010
29 estimates. At individual colonies, the net change was the result of influences of
30 temperature, precipitation and relative humidity change, with smaller effects of
31 wind-speed changes. The largest increases in NH₃ emissions (mean: 60% [486 to -
32 50] increase; A2 scenario for 2099 compared with 2010) were found for colonies
33 40°S to 65°N, and may lead to increased plant growth and decreased biodiversity
34 by eliminating nitrogen sensitive plant species. Only 7% of the seabird colonies
35 assessed globally (mainly limited to the sub-polar Southern Ocean) were estimated
36 to experience a reduction in NH₃ emission (average: -18% [-50 to 0] reduction
37 between 2010 and 2099, A2 scenario), where an increase in precipitation was found
38 to more than offset the effect of rising temperatures.

39 **1 Introduction**

40 Several recent studies have reported that seabirds import significant amount of
41 reactive nitrogen (N_r) from the ocean to the land and play an important role in local
42 ecosystem nutrient cycling (Lindeboom, 1984; Blackall et al., 2008; Riddick et al.,
43 2012). Nitrogen in guano excreted by birds changes chemically as it is either
44 incorporated into the soil organic matter, washed from the land surface or is emitted

45 to the atmosphere as either ammonia (NH₃), nitric oxide (NO), nitrous oxide (N₂O)
46 or diatomic nitrogen (N₂).

47 The formation of NH₃ from seabird guano is of particular interest, as NH₃ is a
48 reactive gas that is readily incorporated into local ecosystems (Blackall et al., 2008),
49 causing significant plant growth near to seabird colonies in otherwise nutrient poor
50 regions (Lindeboom, 1984; Anderson and Polis, 1999). However, excess NH₃ can
51 adversely affect the growth and also reduce plants' tolerance to pests, diseases and
52 other environmental stressors (Stulen et al., 1998; Sutton et al., 2008; Sutton et al.,
53 2011). It is well recognized that NH₃ can cause eutrophication and acidification of
54 ecosystems resulting in a reduction of biodiversity (e.g. Sutton et al., 2011). In
55 addition to near-source ecosystems, NH₃ emissions can adversely affect air quality
56 through aerosol formation (Gu et al., 2014) and alter global climate as the aerosols
57 affect the radiative forcing properties of clouds (Croft et al., 2016; Weber et al.,
58 1998).

59 Previous studies have attempted to estimate the NH₃ emissions from seabird
60 colonies globally. Blackall et al. (2007) applied a bioenergetics model, first
61 developed by Wilson et al. (2004), to estimate a global NH₃ emission of 242 Gg
62 NH₃ yr⁻¹ from seabirds. One major shortcoming of this study was that it did not
63 consider the effects of temperature. Ammonia release from a N_r source is highly
64 dependent on temperature though according to Henry's Law and aqueous NH₃-
65 NH₄⁺ equilibria (Nemitz et al., 2001, Zhu et al., 2011, Riddick et al., 2016b). In the
66 case of avian N_r excretion, which is mainly as uric acid, its hydrolysis to produce
67 NH₃ is also both moisture and temperature dependent (Elliott and Collins, 1982).
68 By not taking these interactions into account, the global emissions estimates of
69 Blackall et al. (2007) must be considered as highly uncertain.

70 The effects of temperature on global NH₃ emissions from seabird guano were
71 subsequently explored by Riddick et al. (2012), where the bioenergetics model of
72 Blackall et al. (2007) was adapted using an empirical temperature correction.
73 Riddick et al. (2012) estimated global emissions using a contemporary seabird
74 population database for three scenarios: no temperature dependence (Scenario 1),
75 full solubility dependence according to the thermodynamics of Henry's Law and
76 aqueous ammonium dissociation (Scenario 2) and) a mid-range estimate between
77 Scenarios 1 and 2 (Scenario 3). The total NH₃ emission for Scenario 1 was estimated
78 at 442 Gg NH₃ year⁻¹, with penguins contributing 83% of the overall emissions.
79 When full thermodynamic temperature dependence was assumed (Scenario 2), the
80 total global NH₃ emission from seabirds was much lower at 97 Gg NH₃ year⁻¹, with
81 penguins contributing 63% of the total emissions. Scenario 3 gave an intermediate
82 estimate of 270 Gg NH₃ yr⁻¹. Riddick et al. (2012) considered that Scenario 3
83 represented the best-guess, as they anticipated that temperature was not the only
84 limiting factor, with other environmental variables, such as precipitation and wind
85 speed, also likely to affect NH₃ emission.

86 Even though Riddick et al. (2012) did not account for all environmental factors,
87 they presented the first global map of NH₃ emissions from seabirds, demonstrating
88 the extent to which seabird emission are remote from anthropogenic sources of N_r.
89 Building on the earlier database of Blackall et al. (2007), the revised database by
90 Riddick et al. (2012) spatially resolved 33,255 seabird colonies of 323 species in
91 180 countries. To address the shortcomings of the Riddick et al. (2012) emission

92 estimate, a process-based approach was developed. First proposed by Blackall
93 (2004) and later refined and tested by Riddick et al. (2017), the GUANO model
94 (Generation of emissions from Uric Acid Nitrogen Outputs) is a dynamic mass-
95 flow process-based model that simulates NH₃ losses from seabird colonies at an
96 hourly resolution. The GUANO model was first applied for comparison with high-
97 and low-temporal resolution measurements datasets (e.g. Blackall et al., 2007;
98 Riddick et al., 2014, 2016a) of seabird NH₃ emissions in different parts of the world.
99 The model application showed that the measured percentage of excreted N_r in guano
100 that volatilizes as NH₃ (P_v) could be well reproduced at sub-polar, temperate and
101 tropical seabird colonies by the GUANO model (Sutton et al., 2013; Riddick et al.,
102 2017). The key climatic driver was found to be temperature, with precipitation,
103 relative humidity and wind speed also influencing P_v .

104 The sensitivity of NH₃ emissions to environmental factors, as clearly demonstrated
105 in measurements (Sutton et al., 2013, Riddick et al., 2014, 2016b), suggests that
106 global climate change over time will affect NH₃ emissions from seabird colonies
107 throughout the world. According to the Intergovernmental Panel on Climate
108 Change (IPCC, 2007), average global surface temperature has been estimated
109 increase by between 1.1 and 6.4 °C by 2100, with global average precipitation
110 changing by up to ± 20 %, a broad scale of change that has since been supported by
111 the IPCC 5th Assessment Report (IPCC, 2013). As many colonies of penguins and
112 other seabird species exist in delicately balanced, pristine environments with low
113 anthropogenic emissions, potentially large changes in NH₃ emissions over the next
114 90 years could have a pronounced environmental impact in these remote regions.

115 The present paper describes an adaptation and application of the colony based
116 GUANO model (Riddick et al., 2017) to calculate NH₃ emission estimates from all
117 seabird colonies detailed in the global seabird database collated by Riddick et al.
118 (2012). The model output provides a new best estimate of current global NH₃
119 emissions from seabirds and a new spatial distribution of emissions which we
120 compare with our previous estimates. We then apply the model using temperature,
121 precipitation, relative humidity and wind speed anomalies for a selection of 2099
122 climate scenarios from IPCC (2007) as a basis to assess how future climate change
123 may affect the distribution and global magnitude of seabird NH₃ emissions.

124 **2 Methods & Materials**

125 **2.1 GUANO Model**

126 For each seabird colony in the global seabird population database (Riddick et al.,
127 2012), we applied the GUANO model (Riddick et al., 2017), using data on
128 meteorology and bird metabolism to calculate hourly NH₃ emissions (F_H , g NH₃ m⁻²
129 h⁻¹) for a period of two years. A two-year simulation was used to calculate the
130 annual emission (F_T , g NH₃ m⁻² year⁻¹) as the sum of hourly emissions for the second
131 year. In this way, the model was able to take account of uric acid deposited in the
132 previous year that has not volatilized or been washed off by precipitation during
133 winter and wet seasons (Blackall et al., 2008). A one-year spin-up time was used
134 because at the colonies where guano builds up, there is either insufficient water to
135 convert uric acid to TAN or it is not warm enough for the TAN to volatilize. In
136 both cases NH₃ emission does not increase in the 3rd year as the meteorology is
137 repeated, with dry climates remaining dry and cold climates staying cold.

138

139 The GUANO model, which is described in detail by Riddick et al. (2017), was
140 converted from a single-site based application (originally implemented in Microsoft
141 Excel) to a script in R to enable large numbers of colonies to be processed at an
142 hourly time resolution. Each colony was simulated independently of the others, i.e.
143 there was no influence in the model of one colony on another.

144 2.2 Model Input

145 2.2.1 Nitrogen excretion rates

146 The average nitrogen excretion rate (N_e , g m⁻² hour⁻¹) for each seabird species used
147 in the GUANO model is calculated from the period of attendance at the colony (T ,
148 days), the proportion of the time spent at the colony during the breeding season (f_{tc}),
149 the number of breeding adults per square meter (D_A , birds m⁻²), the amount of
150 nitrogen excreted per breeding adult (F_{e-br} , g bird⁻¹ day⁻¹), the amount of nitrogen
151 excreted per chick (F_{e-ch} , g chick⁻¹ year⁻¹) and the productivity of the species (P ,
152 fledged chicks per breeding pair).

$$153 \quad N_e = \frac{(1.167T f_{tc} F_{e-br} D_A) + \left(F_{e-ch} \left(\frac{P}{2}\right) D_A\right)}{24T} \quad (1)$$

154 The amount of nitrogen excreted per breeding adult (F_{e-br} , g bird⁻¹ day⁻¹) and the
155 amount of nitrogen excreted per chick (F_{e-ch} , g chick⁻¹ year⁻¹), Equation 2 and
156 Equation 3, are calculated using the method of Wilson et al. (2004) from the adult
157 mass (M , g bird⁻¹), the mass of the chick at fledging ($M_{fledging}$, g), nitrogen content
158 of the food (F_{Nc} , g N g⁻¹ wet mass), energy content of the food (F_{Ec} , kJ g⁻¹ wet mass),
159 assimilation efficiency of ingested food (A_{eff} , kJ [energy obtained] kJ⁻¹ [energy in
160 food]).

$$161 \quad F_{e-br} = \frac{9.2 \cdot M^{0.774}}{F_{Ec} A_{eff}} F_{Nc} \quad (2)$$

$$162 \quad F_{e-ch} = \frac{28.43 M_{fledging}^{1.06}}{F_{Ec} A_{eff}} F_{Nc} \quad (3)$$

163 F_{Nc} and F_{Ec} , estimated at 0.036 g N g⁻¹ and 6.5 kJ g⁻¹ (both wet mass), (Energy:
164 Nitrogen (E:N) ratio = 181 kJ g N⁻¹) respectively, have been calculated assuming a
165 high protein, fish only diet (Furness, 1991). A_{eff} is estimated at 0.8 (Furness, 1991).

166 Species-specific values for input parameters (adult mass, number of days spent at
167 the colony per year, proportion of time at the colony, breeding success, fledging
168 mass of the chick and breeding substrate) were extracted from the literature and are
169 summarised in Appendix 1 of Riddick et al. (2012). Of the 318 species of seabird
170 considered, species specific parameter data were available for 311 species (Birdlife
171 International, 2017). Data for the missing species were estimated from similar
172 species identified using Birdlife International (2017).

173 In its present form, as used in this paper, the global seabird database of Riddick et
174 al. (2012) includes an updated population estimate (261 million breeding pairs,
175 including data from 1984 to 2010). The database details seabird colonies at 33,255
176 locations, with the resolution of colony counts and details varying greatly between
177 countries, from 878 colonies described for the UK (Scotland, Wales, Northern

178 Ireland and England) to a single summary country population values for each of
179 Nigeria, Uruguay and Haiti. As these different levels of detail in the data cannot
180 easily be shown graphically, the maps in the results section aggregate up to a five
181 degree resolution.

182 **2.2.2 Parameterization of hourly air temperature**

183 To calculate NH₃ emission accurately, the GUANO model requires hourly values
184 for air temperature. For the reasons described in Supplementary Material Section
185 1, this study used a model based on Parton and Logan (1981) to calculate diurnal
186 changes in air temperature given a maximum and minimum value. This temperature
187 model calculates the air temperature at 2 m above the surface for each hour day (H)
188 from the day of year (D), latitude (L , °), maximum temperature (T_{max} , °C) and
189 minimum temperature (T_{min} , °C), using a sinusoidal relationship (Parton and Logan,
190 1981). A comparison of the diurnal air temperatures derived from Parton and Logan
191 (1981) with measured values is presented in Supplementary Material Section 1.

192 **2.2.3 Meteorological data**

193 The GUANO model requires hourly input data for ground temperature, relative
194 humidity, wind speed and precipitation. Data from the National Climatic Data
195 Center (NCDC) Global Surface Summary of the Day (GSOD) data (NCDC, 2011)
196 was used as it matched most closely to the data observed during the measurement
197 campaign of Riddick et al. (2014; 2016a) (Supplementary Material Section 2). The
198 daily average values presented in the GSOD dataset were used for relative humidity
199 and wind speed. Hourly values for precipitation were calculated from the daily total
200 divided by 24. Hourly air temperature values were calculated from the daily
201 maximum and minimum using the method described above in 2.2.2, ground
202 temperature data are not readily available and, therefore, were derived from air
203 temperature, as described in Section 2.2.4.

204 **2.2.4 Ground Temperature Modelling**

205 In the absence of suitable global data for ground surface temperature
206 (Supplementary Material Sections 2 & 3), this was derived from air temperature
207 data for each colony, using surface and air temperature data from the three field
208 work sites measured during the campaigns of Riddick et al. (2014, 2016a) to
209 parameterize a temperature offset (T_o) function (Supplementary Material Section
210 3). For each seabird colony, T_o was calculated from the difference between air and
211 ground temperatures measured during field campaigns at: the equator = T_o
212 (Ascension Island; Riddick et al., 2014), 55 °N = T_o (Isle of May; Riddick et al.,
213 2016a) and 55 °S = T_o (Bird Island; Riddick et al., 2016a). Using these
214 measurements, T_o was derived for each seabird colony at each hour at any given
215 latitude based on linear interpolation between latitudes of these hourly values.

216 Due to the relatively simple derivation method and the limited number of
217 measurement sites, there is substantial uncertainty associated with the estimated
218 surface temperature. Based on daily variations in ground temperature at the three
219 measurement sites, a best estimate of uncertainty in derived ground temperature at
220 these sites is ± 1 °C. However, the global interpolation of these values must be
221 acknowledged to be more uncertain, and probably ± 2 °C as a best estimate.

222 **2.2.5 Assigning meteorological stations to seabird colonies**

223 The geographically closest meteorological data in the GSOD database to each
224 seabird colony were identified and extracted using a GIS. These meteorological
225 data were used in the GUANO model to calculate NH₃ emissions for a base year of
226 2010. For colonies farther than 1000 km from a measurement site, the
227 meteorological data were calculated as the average of the nearest three sites. The
228 cut off of 1000 km was used because it was assumed that, for our purposes, climate
229 at sea level would be sufficiently similar to sites within this distance. This
230 correction was only necessary for 50 colonies out of the total of 33,255 colonies
231 (<0.2%), mostly in the South Pacific and around Antarctica.

232 **2.3 Analysis of meteorological effects**

233 In order to investigate the relative effects of meteorology on NH₃ emission,
234 relationships were fitted using a multiple regression model. Correlations between
235 NH₃ emissions and the hourly meteorological data for each variable (air
236 temperature, relative humidity, wind speed and precipitation as presented in the
237 GSOD dataset) were identified by calculating the product moment correlation
238 coefficient (*r*).

239 **2.4 Climate change scenarios**

240 Data from the IPCC Special Report on Emissions Scenarios (IPCC, 2007) were
241 used to simulate potential future changes in NH₃ emissions from seabirds for
242 different climate change scenarios. The specific scenarios used were: the best-case
243 scenario (B1), the middle scenario (A1B) and the worst-case scenario (A2) (Mann
244 & Kump, 2008). Scenario-specific data are available from the IPCC data
245 distribution centre (IPCC Data, 2017) and were chosen because it provided anomaly
246 data on temperature, northward and eastward wind components, precipitation and
247 humidity for 2099 on a 2.5° by 3.75° grid.

248 The geographically closest anomaly data for each seabird colony were extracted
249 using a GIS and added to the meteorological data in the GUANO model for the year
250 2099. It should be noted that no account was taken of potential effects of climate
251 change on seabird populations that might occur due to changes in food availability
252 or physical changes to breeding sites, e.g. sea level rise or increased storm
253 frequency.

254 **3 Results and Discussion**

255 **3.1 Global distribution of seabird NH₃ emission**

256 The GUANO model application based on 2010 estimated total NH₃ emission at 81.8
257 Gg NH₃ year⁻¹, with large emissions in hotspots throughout the world, especially on
258 tropical and sub-polar islands (Figure 1). It may be noted from Figure 1 that seabird
259 species sometimes occur inland, for example cormorant colonies in Central Asia.
260 The resulting distribution may be compared with the three empirical scenarios of
261 temperature dependence mapped by Riddick et al. (2012): emissions assumed to be
262 independent of temperature (Scenario 1: 404 Gg NH₃ year⁻¹), emissions assumed to
263 follow thermodynamically adjusted bioenergetics (referred to subsequently as the
264 TABE model) (Scenario 2: 83 Gg year⁻¹) and the mid-estimate between these two
265 (Scenario 3: 244 Gg year⁻¹). Overall, the GUANO model is found to agree most
266 closely with the TABE model estimate of Riddick et al. (2012) (Scenario 2),

267 pointing to a lower estimate of global emissions than what their best guess (Scenario
268 3). This similarity to Scenario 2 should, however, be considered as partly fortuitous,
269 since the GUANO model uses a process based approach, compared with the
270 empirical fit to measurements of Riddick et al. (2012), which does not include the
271 effects of precipitation, relative humidity and wind. The consequence is that the
272 spatial patterns of NH₃ emission across the world are also very different between
273 this new dataset and the TAFE model results.

274 Geographically, the main differences between the GUANO model and the TAFE
275 model are for the sub-polar latitudes (40 °S - 60 °S), where the TAFE model
276 emissions are twice as large as the GUANO model emissions (Supplementary
277 Material Section 5 Figure SM5.1). These emissions are generally from the penguin
278 colonies in the Southern Ocean, where temperatures are relatively low and
279 precipitation is high, and the difference may be caused by unvolatilized nitrogen
280 remaining on the ground longer before it is washed away by precipitation.

281 Between 15 °N and 25 °S, NH₃ emissions calculated by the GUANO model are
282 higher than those calculated by the TAFE model (Supplementary Material Section
283 5 Figure SM5.1). Both models incorporate an exponential relationship between
284 temperature and NH₃ emission. However, the larger emissions in the tropics may
285 be caused by the use of hourly ground temperature values in the GUANO model
286 instead of an average value for the breeding season in the TAFE model. The peaks
287 during the day result in a higher P_v and exponentially larger emissions which are
288 reflected in the larger annual emissions and average P_v (average tropical P_v for the
289 GUANO model is between 10 and 15% higher than the average tropical TAFE
290 model P_v) at seabird colonies in the tropics (Supplementary Material Section 5
291 Figure SM5.1).

292 <<Insert Figure 1>>

293 A detailed comparison of the estimates from the GUANO and TAFE models for 13
294 regions of the world is given in Supplementary Material Section 4 (Table SM4.2).
295 Generally, NH₃ emissions calculated by the GUANO model are larger than the
296 TAFE model from colonies in the tropics in areas such as Australasia (72% larger)
297 and the Indian Ocean (117% larger). However, NH₃ emissions calculated by the
298 GUANO model are smaller than the TAFE model from colonies in colder, wetter
299 areas, such as Antarctica (35% smaller). As noted above, this is caused by the
300 GUANO model taking into account nitrogen wash-off from the colony as a
301 consequence of precipitation. The largest regional difference between the TAFE
302 and GUANO modelled NH₃ emissions is in Asia where the GUANO model predicts
303 emissions 4.8 times larger. The TAFE and GUANO model emissions were
304 calculated using the same input bird data and the most noticeable difference in
305 emissions is in the colonies around the Sea of Okhotsk (Supplementary Material
306 Section 5 Figure SM5.3). As explained above, the exponential relationship between
307 temperature and NH₃ emission in the GUANO model uses hourly values of ground
308 temperature, resulting in exponentially larger emissions. As the TAFE model uses
309 average temperature during the breeding season rather than daily varying
310 temperature, the exponential relationship would tend to give higher emissions in the
311 GUANO model in the warmest areas.

312 **3.2 Analysis of meteorological effects on NH₃ emissions**

313 The relationships of temperature, relative humidity, wind speed and precipitation
314 were compared to the P_v estimates derived from the GUANO model for the breeding
315 season at all global colonies (Supplementary Material Section 5 Figure SM5.3).
316 Given that there is no strong correlation between the different meteorological
317 variables themselves (Supplementary Material Section 5 Table SM5.1), we applied
318 a multiple regression model to establish their relative importance to P_v . The multiple
319 regression model between meteorological parameters is based on averaged values,
320 where daily averaged data was used as hourly data for relative humidity and wind
321 speed. Hourly precipitation is the daily total precipitation divided into 24 equal
322 hourly values and the hourly temperature is the hourly ground temperature as
323 calculated by the method in Supplementary Material Section 3. The multiple
324 regression model indicates that, modelled across the sites, P_v is most sensitive to
325 temperature and precipitation (Supplementary Material Section 5 Table SM5.2).
326 Warmer conditions favour an increase in P_v , while wetter conditions, which
327 includes the effects of relative humidity, with more precipitation favour a smaller
328 P_v . Wind speed has the least effect on P_v of the four variables included, however
329 the relationship is positive and wind speed clearly affected measured emissions at
330 some sites, especially Bird Island (Riddick et al., 2016a). In strong winds, both
331 aerodynamic and boundary-layer resistances are reduced and the rate of emission
332 increases. However, wind speed only limits the rate of transport of NH₃ from the
333 ground and the magnitude of wind speed has no effect on the rate of NH₃
334 production.

335 The relationships between meteorological variables and P_v can be explained by
336 considering how uric acid evolves to form NH₃. Ammonia emission increases with
337 temperature because of decreased solubility of NH₃ on the surface described by
338 Henry's Law. The TABE model does not take into account uric acid, TAN and non-
339 volatilized NH₃ washed away during precipitation events. It is difficult to
340 parameterize N run-off because of differences in speed and efficiency in wash-off
341 of guano from different nesting habitats (such as rock, sand, burrows) and slopes.
342 Like temperature, increases in relative humidity increase the amount of uric acid
343 that converts to TAN because of increased hydrolysis, which would explain the
344 significant relationship between relative humidity and NH₃ emission.

345 The effects of meteorology on P_v can explain why the global seabird NH₃ emission
346 calculated using the GUANO model is lower than previous estimates. The TABE
347 model (Riddick et al., 2012 - Scenario 2) estimates that 65 % of global NH₃
348 emissions are due to penguin species, compared with 42% according to estimates
349 using the GUANO model. This smaller contribution by penguins can be explained
350 by temperature reducing the amount of NH₃ evolved from uric acid at these sites.
351 Due to the penguin colonies' location on cold and wet Sub-Antarctic islands, TAN
352 is formed only slowly from uric acid, resulting in low NH₃ emission rates. Coupled
353 with this, precipitation events reduce the presence of uric acid, TAN and NH₃ at the
354 surface due to run-off, thereby decreasing the overall percentage of excreted
355 nitrogen that is available for volatilization.

356 The largest populations of seabirds are found in Antarctica and the Southern Ocean,
357 and because of their relatively large mass, these are also the species excreting the
358 most nitrogen (Riddick et al., 2012). On a global scale, seabird N excretion is

359 dominated by Antarctica and the Southern Ocean, which account for 79 % of the
360 total excreted. However, the meteorology (low temperatures and high precipitation)
361 at these colonies reduces emissions to relatively small values, thus only 34.2 Gg
362 $\text{NH}_3 \text{ year}^{-1}$ are emitted from the 858.2 Gg N year^{-1} excreted in Antarctica and the
363 Southern Ocean ($P_v = 4 \%$) (Figure 2). By contrast, NH_3 emissions from the tropics
364 are relatively high compared with the total amount of N excreted, mainly due to hot
365 temperatures. For example, seabird colonies on the Pacific islands emit 13.0 Gg
366 $\text{NH}_3 \text{ year}^{-1}$ from the 29.7 Gg N year^{-1} excreted ($P_v = 44 \%$) (Figure 2).

367 It is similarly important to note the importance of water availability, both through
368 precipitation and relative humidity is parametrized in the GUANO model. In
369 conditions where NH_3 emission is restricted by low relative humidity e.g. Ascension
370 Island (Riddick et al., 2014), higher precipitation increases the water budget of
371 guano, increasing uric acid hydrolysis rate to form ammonia and ammonium in
372 solution, (Riddick et al., 2017). Hence some water is needed to allow hydrolysis,
373 which in warm locations promotes a high value of P_v . Conversely, in extremely
374 warm dry locations, lack of hydrolysis leads to low P_v values, and an associated
375 build-up of guano. It is therefore no surprise that Pisco on the west coast of Peru,
376 famous for its guano mining industry, is estimated to have a low P_v value (Figure
377 2) despite high temperatures. In this way, the GUANO model could also be used
378 to simulate the accumulation of guano as a resource and the influence of climate
379 change on this resource.

380 By contrast, the highest P_v value of any seabird colony in our model was found for
381 on Wake Island in the South Pacific (19.27°N, 166.64°E), where the annual mean
382 temperature is 27°C, with an annual average precipitation of 906 mm and relative
383 humidity of 95%. At this a site, the hydrological conditions, modest precipitation
384 and high humidity, means the hydrolysis of the excreted uric acid is maximized,
385 with the high temperatures in turn maximizing the fraction of TAN that volatilizes
386 rather than runs-off into the sea.

387 <<Insert Figure 2>>

388 **3.3 Simulated effects of climate change on emissions**

389 The application of the GUANO model for 2099 allows the effects of future climate
390 change scenarios to be assessed. A comparison with the 2010 baseline shows that
391 NH_3 emissions could increase substantially through the influence of climate on P_v
392 alone, assuming no change in seabird populations and breeding success (Table 1).
393 Given the associated complexities, however, predicting how seabird populations
394 change in the future with anticipated changes in global climate is beyond the scope
395 of the current study. Using nitrogen excretion rates of 2010, increases in NH_3
396 emission are estimated here in the region of 22-32 Gg $\text{NH}_3 \text{ year}^{-1}$ for the IPCC
397 Scenarios B1, A1B and A2 (Table 1). This amounts to a climate change driven
398 increase in emissions of around 26 to 39% between 2010 and 2099, depending on
399 the scenario used.

400 <<Insert Table 1>>

401 The spatial distribution of increases and decreases to the 2010 estimated values of
402 P_v , based on the worst case (A2) data set is presented in Figure 4. To test the effects
403 of predicted wind speed changes separately from changes to the other variables, the
404 wind speed anomalies were added to the GSOD wind dataset and show that wind

405 speed changes in 2099 have little effect on modelled NH₃ emission globally, <5%
406 at colonies with the largest predicted change (Figure 3a). When the A2 anomalies
407 for relative humidity alone are added to the GSOD dataset, the effects on P_v are
408 much larger, ranging from -17% to +22% (Figure 3b). The largest estimated
409 increases in P_v associated with future relative humidity are in tropical regions of the
410 world, with P_v increasing by up to 22% on many islands in the Indian and Pacific
411 Oceans (Figure 3b). These are regions where guano mining has been conducted,
412 and even relatively small increases in moisture (relative humidity) to these areas
413 may result in an increase in NH₃ loss at these sites and provide a potential threat to
414 the quality and levels of guano production.

415 <<Insert Figure 3>>

416 Precipitation anomalies can act to either increase or decrease P_v with P_v increasing
417 by up to 130 % at colonies where precipitation decreases, such as Norfolk Island,
418 due to less wash-off (Figure 3c) and decreasing by up to 45 % on Pacific Islands.
419 Increases of P_v between 1 and 10 % are estimated throughout Europe, the Caribbean
420 and the Pacific. P_v decreases (linked to increased precipitation) are estimated for
421 most of the regions with colder climates, including Sub-Antarctic Islands and the
422 Arctic.

423 Increases in P_v are most obvious for the predicted A2 temperature anomalies (Figure
424 3d). The regions with the largest increases (20 - 29 %) are mainly around the
425 Mediterranean and North East Russia. However, in the coldest regions (Sub-
426 Antarctic and Arctic), there may be little or no increase to P_v

427 When the influence of all A2 climate anomalies together is considered, the largest
428 changes to P_v are predicted for the hottest climates, including the Pacific Islands,
429 Indian Ocean islands, Australia and the Mediterranean (Figure 4). These large
430 increases in P_v are expected by the amplifying effect of temperature and water
431 availability from relative humidity and precipitation. The P_v is not predicted to
432 change substantially in the colder climates of the Sub-Antarctic Islands and around
433 the Antarctic peninsula because of relatively negligible increases in temperature
434 (Supplementary Material Section 6 Figure SM6.1).

435 <<Insert Figure 4>>

436 The effects of climate change on P_v at the largest seabird colonies in the world (by
437 number of seabirds) are shown in Figure 5 and Supplementary Material Section 6
438 Tables SM6.1 and Figure 3 (the location of each of these colonies is presented in
439 Supplementary Material Section 6 Figure SM6.2). Ammonia emissions from the
440 penguin colonies on the Isles Kerguelen and Willis Island are predicted to be largely
441 unaffected by climate change (<5% change), even in the worst-case scenario (A2).
442 This is due to increased precipitation balancing out increased temperatures, as
443 discussed above. At colonies with a large increase in precipitation (e.g. the colonies
444 on the South Sandwich Islands), NH₃ emissions are predicted to decrease because
445 the increased precipitation is likely to wash excreted nitrogen from the colony
446 before it can be emitted as NH₃. Colonies with predicted temperature increases and
447 precipitation decreases (e.g. the Rockhopper penguin colony on Tristan da Cunha),
448 show the largest predicted increase in NH₃ emissions, due to the coupled effect of
449 a decrease in uric acid wash-off because of decreased precipitation and the
450 increased surface NH₃ concentration. Note that the highest volatilization rate for

451 any major colony shown on Figure 5 is on the Peruvian Island of Lobos de Tierra
452 (6.39 °S, 80.85 °W), where 69% of the excreted nitrogen is estimated to be
453 volatilized, increasing in 2099 to 73%. This may be contrasted to guano harvesting
454 areas near Pisco on the west coast of Peru (latitude 14 °S, Supplementary Material
455 Figure SM6.2) where P_v is estimated to increase from 25% to 56% under between
456 2010 and 2099, indicating the potential to affect future guano production.

457 <<Insert Figure 5>>

458 **3.4 Evaluation in comparison with measurements**

459 While the main focus of this paper is on assessing the climate dependence of NH_3
460 emissions and their potential to change under future climate change scenarios, it is
461 important to reflect on the extent of model validation. While it is not feasible to
462 check the modelled emissions from seabird islands on a global scale, the GUANO
463 model has been subject to verification for a number individual colonies across
464 different climates. This is illustrated in Figure 6, which compares (a) the area-based
465 NH_3 emission value and (b) the P_v value calculated by the GUANO model to
466 matching values derived from measurements. Further details of the site based
467 comparison with measurements and methods used to calculate the uncertainty in
468 emission are provided by Riddick et al. (2014; 2016a; 2017).

469 In principle, the GUANO model was developed independently of the field
470 measurements, except the habitat correction factors. The GUANO model emission
471 estimates match the measurements more closely than the emission calculated by
472 Riddick et al. (2012) for both area-based emission ($R^2 = 0.75$, $m = 0.80$, $p\text{-value} =$
473 0.057) and P_v ($R^2 = 0.91$, $m = 1.07$, $p\text{-value} = 0.01$), as the model accounts for the
474 effect of both thermodynamics and the nitrogen depletion through precipitation
475 events. Where the measured emissions are higher than those calculated by the
476 GUANO model (Ascension Island and the Isle of May), this may reflect that the
477 measurements were taken during the breeding season, which is generally the hottest
478 time of the year and when there is the most available nitrogen, and the GUANO
479 model emissions are the average of a year-round simulation.

480 Also presented are the area-based NH_3 emission value and the P_v value
481 (Supplementary Material Section 6 Figure SM6.3) calculated by Scenario 1
482 (bioenergetics model), Scenario 2 (temperature adjusted bioenergetics model) and
483 Scenario 3 (best estimate) of Riddick et al. (2012). Generally, the BE model
484 emission estimates are too high in colder areas (Bird Island and Signy Island) and
485 too low in hotter areas (Michaelmas Cay and Ascension Island) and have poor
486 agreement when compared against area-based emission estimates ($R^2 = 0.15$, $m =$
487 -3.94 , $p\text{-value} = 0.52$) and P_v ($R^2 = 0.45$, $m = -0.31$, $p\text{-value} = 0.21$). This is partially
488 addressed by using the thermodynamic correction of the TABE model, when
489 compared against area-based emission ($R^2 = 0.08$, $m = -0.51$, $p\text{-value} = 0.64$) and P_v
490 ($R^2 = 0.92$, $m = 0.19$, $p\text{-value} = 0.01$), however this does not account for the full
491 effects of the meteorology on the biogeochemical processes, i.e. the difference
492 between the P_v for the GUANO and TABE models in Figures SM6.4 and SM5.1
493 will partly be a result of direct measurement of temperature instead of using an
494 average annual temperature.

495 <<Insert Figure 6>>

496 **3.5 Uncertainty in input data**

497 The meteorological parameters used as input to the GUANO model are a major
498 source of uncertainty, especially the calculation method for ground temperature.
499 The estimated ground temperature used in the GUANO model is based on average
500 ground temperature variations at the three main field measurement sites of Riddick
501 et al. (2014, 2016a). An uncertainty estimate of ± 2 °C was estimated. This results
502 in an NH₃ emission uncertainty of ± 32 % at best. Additionally, precipitation data
503 may also have some associated uncertainty as the reported precipitation data at
504 many colonies is very low (Supplementary Material Section 5 Figure SM5.3) which
505 may result in either underestimation of NH₃ emission through lack of water to form
506 uric acid or overestimation as not enough run-off is accounted for.

507 However, another substantial uncertainty in global NH₃ emission is the seabird
508 population estimate (± 36 %) (Riddick et al., 2012). New counting techniques have
509 resulted in increased estimates of seabird populations counted in the most remote
510 regions. For example, remote sensing was used to count Little auks (*Alle alle*) on
511 Northumbria Island, Greenland (Egevang et al., 2003), computer-based analysis
512 was applied to count Macaroni penguins in colour aerial photographs on Bird
513 Island, South Georgia (Trathan, 2007), and super-high resolution satellite imagery
514 was used for a census of threatened albatrosses in remote regions (Fretwell et al.,
515 2017). However, because seabirds are generally difficult to reach and new methods
516 are expensive, a large uncertainty in population estimates remains. Combining the
517 sources of error provides a global best estimate of NH₃ emission from seabird
518 colonies of 82 [37 - 127] Gg NH₃ year⁻¹.

519 **3.6 Uncertainties in simulated emissions.**

520 The GUANO model provides a method for calculating NH₃ emission from a range
521 of climates. A major asset of the GUANO model is its relative simplicity. For
522 example, it was easily adapted from a site-based approach (Riddick et al., 2017) to
523 model NH₃ emissions for all colonies globally using hourly time-steps for a two
524 year period. Conversely, the simplicity of the GUANO model does impose some
525 limitations. The model uses basic expressions to calculate vertical dispersion at the
526 colony, while complex local topography will influence wind speeds and local
527 turbulence. To ascertain if complex topography has a large effect on NH₃ emission,
528 the model should be validated with NH₃ emissions from colonies with more
529 complex aerodynamics. While this is likely to affect simulated emissions in cold
530 climates where, as Riddick et al. (2014, 2016a) show, emissions are to some extent
531 wind speed dependent, this is likely to be less important in warm climates which
532 are more strongly affected by variability in temperature and water availability.

533 Many seabird colonies are low lying (e.g., Michaelmas Cay is only 3.5 m above
534 sea-level) and the potentially volatilizable nitrogen may be washed away by storms
535 washing over the land. Until now, wash-off by storm action (i.e., the combined
536 action of wind and water) has been omitted from the GUANO model, which only
537 includes a simple parametrization as a function of precipitation amount. However,
538 the effect of storms could be modelled with the inclusion of colony height above
539 sea level and a relationship between wind speed and wave height. This would
540 require detailed high-resolution digital elevation data for colonies, as some sites are
541 at risk in their entirety, whereas only the lower parts of steeper sloping sites or cliffs
542 would be at increased risk from storms. The slope of a site would also be a key

543 parameter for calculating wash-off by precipitation during and between breeding
544 seasons. However, the spatial resolution of the global seabird database is currently
545 insufficient for all parts of the globe, with data from some countries not being
546 available at the individual colony level. However, in general, the colonies with the
547 poorest spatial resolution are the smallest colonies with smaller contribution to the
548 total seabird NH₃ emission.

549 The effects of different forms of precipitation on NH₃ emission are not included in
550 the GUANO model. It could be anticipated that colder forms of precipitation (hail,
551 sleet and snow) could affect the temperature of the system and slow the rate of NH₃
552 formation. Higher intensity of precipitation events may encourage wash-off, as
553 torrential rain may cause flooding events while a similar volume of drizzle over a
554 longer time period may be absorbed into the surface with less wash-off. Global
555 rate/temperature of precipitation data are not known to exist, but the model could
556 be developed in future iterations to account for cold or intense precipitation events
557 if data were available, or by implementing proxy information such as air
558 temperature.

559 While it is acknowledged that the GUANO model still has weaknesses in the
560 representation of run-off and wash-off by precipitation and storms, it reproduces
561 measured NH₃ emissions at the study sites well (Figure 6 and Riddick et al., 2017).
562 The further refinements suggested above could help to gain better understanding of
563 NH₃ emissions, particularly in regions with high precipitation and storm frequency,
564 and for exploring the extent to which sea level rise may affect colonies.

565 In addition to parameterization, there may be further uncertainty the absolute NH₃
566 emission predicted for 2099 caused by guano build up at the colony that is not
567 accounted for by the GUANO model. For the 2010 scenario at the colonies with
568 guano build up, there is either insufficient water to convert uric acid to TAN or it is
569 not warm enough for the TAN to volatilize. In both cases NH₃ emission does not
570 increase in the 3rd year as the meteorology is repeated, with dry climates remaining
571 dry and cold climates staying cold. For the 2099 scenario the NH₃ emission
572 estimate could be an underestimation at colonies that were dry, but then experience
573 higher precipitation. In these cases, accumulated guano not accounted for by the
574 GUANO model will form “historic” NH₃ from residual guano as well as “present-
575 day” NH₃ from freshly excreted guano. To make a justifiable estimate on the NH₃
576 emissions from historic guano the model would need to run from at least the present
577 day. The first problem with this is we do not have the processing power to do this
578 as the GUANO model takes 24 hours to run for 1 year. Also, changes in seabird
579 population could lead to incorrect emission estimates as NH₃ emissions from
580 recently abandoned penguin rookeries had similar emissions to that of occupied
581 colonies (Speir and Ross, 1984). In a wet temperate climate, Blackall et al. (2008)
582 found ammonia emissions to return to zero within 1-2 month of birds departing,
583 with no carry-over of guano or emission to the following year. Despite the
584 shortcomings of the 2099 NH₃ emission prediction, the P_v is unaffected by historic
585 guano emissions. The colony specific P_v is presented as a more significant outcome
586 than the absolute emission as the absolute emission will also be affected by our
587 highly uncertain values of seabird population in 2099. Future work could compare
588 simulated surface uric acid or TAN from GUANO with field observations as this
589 could be a useful way to assess how well pre-deposited guano is simulated by the
590 model.

591

592 **3.7 Implications of the research**

593 **3.7.1 Comparison of global emissions with other estimates**

594 It is important to summarize the main reasons for the differences between the
595 GUANO model estimate of global NH_3 emissions ($82 \text{ Gg NH}_3 \text{ year}^{-1}$) and the other
596 published estimates. The present study and its validation by measurements clearly
597 shows that the estimates of Blackall et al. (2007) and Riddick et al. (2012, Scenarios
598 1 and 3) are too high, which is mainly because volatilization rates in polar regions
599 are limited by cold temperatures with substantial amounts of run-off. In simulating
600 NH_3 emissions from grazing animals, Móríng et al. (2016) recently demonstrated a
601 feature that may also be relevant to better understand NH_3 emissions from seabird
602 colonies: lower temperatures lead to smaller instantaneous emissions, but as
603 ammoniacal nitrogen remains at the surface this increases the potential for NH_3
604 emissions at a later stage, thereby increasing the duration of emissions. In this way,
605 if it were not for other loss pathways and interactions, temperature would not
606 ultimately affect the total amount of NH_3 emitted. It is then the interaction between
607 temperature, emission timescale and other competing processes (such as run-off)
608 that lead, in practice, to temperature dependence of NH_3 emission. In the context of
609 the GUANO model, run-off refers to the leaching of TAN and uric acid into the
610 substrate or lateral transport into the sea and is no longer considered
611 biogeochemically available for NH_3 emission. With cooler conditions, and lower
612 instantaneous NH_3 emissions, this increases the chance that the N_r will be washed
613 off by a precipitation event rather than emitted to the atmosphere.

614 A major consequence of the lower NH_3 emission calculated in this paper is the
615 change this makes to understanding nitrogen pathways at a colony level.
616 Lindeboom (1984) estimated that the percentage of excreted nitrogen that
617 volatilizes (P_v) could be 80 % at a Macaroni penguin colony on Marion Island
618 (Southern Ocean, 47°S , 38°E). By contrast, a value of 1.7 % P_v is estimated for
619 the Macaroni penguin colonies on Bird Island using the GUANO model (54°S , 38°W)
620 (Supplementary Material Section 6 Figure SM6.2) which is supported by a
621 measurement-based estimate of 1.8% at the same site. This large difference in P_v
622 cannot be explained by taking into account the 2°C higher average temperature
623 during the breeding season at Marion Island (NCDC, 2011). In the global GUANO
624 model application we included Marion Island as one of the sites, where the annual
625 P_v value is estimated at 3%, which is consistent with our measurements and site
626 based simulations at Bird Island. Lindeboom (1984) estimated P_v by comparing
627 nitrogen and phosphorus ratios in fresh excreta to older excreta at the colony,
628 assuming that nitrogen was only lost by volatilization, but did not consider nitrogen
629 loss by run-off, which would explain their over-estimation in P_v for Marion Island.

630 In contrast to the low P_v for penguin colonies, our measurements found that 67 %
631 of the excreted N_r volatilizes as NH_3 at the seabird colony on Michaelmas Cay
632 (Riddick et al., 2014). This compares with a simulated value using the GUANO
633 model for the measurement period of 82% (Riddick et al., 2014), while our global
634 GUANO model application here for gives an annual average P_v of 69%. Our
635 measurements and modelling thus support the early Lindeboom (1984) estimate,
636 but only in colony situations where volatilization dominates with negligible run-off.

637 **3.7.2 Magnitude and significance of seabird NH₃ emissions**

638 The magnitudes of NH₃ emissions calculated by the GUANO model indicate that
639 seabird colonies represent appreciable local NH₃ sources compared with the better
640 known agricultural sources of NH₃ emissions. For example, a poultry installation
641 of similar NH₃ emission as Michaelmas Cay (8,672 kg NH₃ year⁻¹) would house
642 80,000 birds, with each bird emitting NH₃ at 0.1 kg NH₃ bird⁻¹ year⁻¹ (Sutton et al.,
643 2011). This is similar to the emission from a cattle feedlot of over 650 animals
644 emitting ~10.4 kg NH₃ animal⁻¹ year⁻¹ (Sutton et al., 2011). The largest source of
645 NH₃ emission in our global model for 2010 is Baker Island in the South Pacific
646 (0.19°N, 176.48°W), which emits 3.9 Gg yr⁻¹ (equivalent to the emissions of 39
647 million chickens or 375 thousand cattle). For 2099 (Scenario A2), our global model
648 still predicts Baker Island to emit the largest amount of NH₃, but this has increased
649 to 6.7 Gg yr⁻¹.

650 Wilson et al. (2004) reported that UK seabird colonies in remote regions are
651 significant local sources of NH₃ where other emission sources are scarce. At a
652 global scale, seabird colonies are even more removed from anthropogenic nitrogen
653 sources and in many locations can be considered the only major atmospheric
654 nitrogen deposition source for nearby terrestrial ecosystems. This spatial isolation
655 of seabird NH₃ emissions from anthropogenic sources can be put into context by
656 comparison with the spatial estimates of NH₃ emissions from other sources as
657 included in the EDGAR database (EC-JRC/PBL, 2010). When the 0.1° x 0.1° NH₃
658 emissions in the EDGAR database are co-located with the seabird NH₃ emissions
659 database at same scale, contributions of NH₃ from seabirds mostly account for more
660 than 99.9 % of NH₃ emissions from all sources within the 0.1° x 0.1° cell where
661 they occur (Supplementary Material Section 7 Figure SM7.1).

662 **3.7.3 Seabirds as a model system to study for global ammonia emissions**

663 Seabirds can be considered as representing a "model system" to study NH₃ emission
664 that can provide insights to understand other sources of NH₃ emission better. Many
665 sources of NH₃, especially in agriculture, are complicated by different management
666 practices, whereas seabird emissions are a natural system, uninfluenced by local
667 differences in management practice. As a result, examination of seabird colonies is
668 especially useful to study the climate dependence of NH₃ emission. In this way,
669 relationships between NH₃ emissions and meteorology can be identified without
670 complications from several externally varying anthropogenic factors (e.g. ground
671 management, manure management techniques, animal housing practices etc.). The
672 GUANO model application presented here provides a step on the way to developing
673 a comprehensive climate-dependent approach to ammonia emissions modelling
674 (Riedo et al., 2002, Sutton et al., 2013, Riddick et al., 2016b) for which parallel
675 steps are being made in other emission contexts (e.g. Bash et al., 2012, Mórning et
676 al., 2016).

677 The present paper shows that NH₃ emissions from seabird nitrogen are highly
678 dependent on meteorology. While an illustrative range for the most important
679 species is shown in Table SM4.1, the full range between species extends from an
680 average P_v of 0.4 % for Emperor penguins to 68.0 % for the Peruvian tern found in
681 South America (see Table 2). While there are differences in emission processes
682 between seabird excreta and animal manure, the principles of the GUANO model
683 are generic and it could be adapted for different types of excreta, such as poultry

684 litter, animal manure and slurry. These adapted models could be used to investigate
685 the dependence of NH₃ emissions from agricultural sources according to
686 meteorology and in consideration of management differences where such data can
687 be obtained.

688 <<Insert Table 2>>

689 **3.8 Climate change relationships**

690 The results presented here suggest major spatial changes in the percentage of
691 nitrogen that volatilizes as a result of global climate change. At seabird colonies
692 where the largest temperatures are predicted (e.g., Tristan da Cunha, South Atlantic
693 and Midway Atoll, Pacific Ocean), we estimate that P_v increases (Figure 4). Higher
694 P_v leads to an increase in NH₃ volatilized, and may result in increased plant growth
695 and decreased biodiversity by eliminating nitrogen sensitive plant species
696 (Lindeboom, 1984; Ellis, 2005). However, at seabird colonies where precipitation
697 is also predicted to increase, greater run-off will also offset the increase in
698 temperature. The net result is the expectation of negligible changes to P_v at some
699 locations, e.g. on Willis Island and Isles Kerguelen in the Southern Ocean.

700 Only a few locations globally are expected to have smaller emissions in 2099 than
701 in 2010 according to Scenario A2. Only 7% of the seabird colonies assessed
702 globally (mainly limited to the Southern Ocean; Figure 4) are predicted to
703 experience a reduction in NH₃ emission. Of this 7%, the largest reduction P_v
704 between 2010 and 2099 (using A2 scenario) was 6.3 % and an average of -1.1%.
705 At these colonies the increase in precipitation was found to more than offset the
706 effect of rising temperatures.

707 An analysis of average values of the change in simulated P_v from 2010 to 2099 as
708 calculated by the GUANO model shows that average P_v values for seabird species
709 in hot climates are predicted to increase by more than 20 %, such as the Sooty tern
710 and the Common noddy (Table 2). Average P_v values for seabirds in temperate
711 climates, such as the Atlantic puffin, are estimated to increase by nearly 5 %. For
712 seabirds in the cold regions, P_v values are predicted to increase by small amounts
713 or decrease, e.g. a decrease in average P_v of 1.2 % for Macaroni penguins. By
714 contrast, for Macaroni penguins located especially in sub-Antarctic areas where
715 precipitation is expected to increase, a small decrease of 1.2% is predicted (Table
716 2).

717 The GUANO model predictions for 2099 only take climate change into account,
718 while assuming that seabird populations will remain stable at their colonies.
719 However, seabird populations, and hence NH₃ emissions, are also expected to be
720 affected by the changing climate. Predicting future population changes in seabirds
721 in response to anticipated climate change was beyond the scope of the present study,
722 but is also relevant for future scenario development.

723 Some of the global changes expected to affect seabird colonies are sea-level rise
724 (0.23 – 0.51 m for the A2 scenario), an increased frequency of extreme weather
725 events, increased frequency in the El Niño Southern Oscillation and increased sea
726 surface temperatures (IPCC, 2007).

727 Sooty terns nesting on low lying atolls in the Pacific Ocean provide an example of
728 how sea-level rise and an increase in the frequency of extreme weather events may
729 affect breeding grounds of seabirds. Michaelmas Cay is currently 3.5 m above sea-

730 level, but with predicted changes in sea-level and more frequent extreme weather
731 events, this land may not be a viable nesting site in the future. 120 days are required
732 between egg-laying and fledging for the species at this site, and changing climate
733 may limit the number of consecutive days the island is above water.

734 An example of the effect of El Niño is the change to the Guanay cormorant
735 populations on the west coast of South America. The El Niño Southern Oscillation
736 occurs when warm water appears off the coast of Peru and results in lower primary
737 production of the oceans (Wyrski, 1975). Past El Niño events coupled with
738 overfishing have had a large impact on the food chain and resulted in a decrease of
739 the Guanay cormorant population in Peru from 20 million in the 1950s (Santander,
740 1981) to 3 million in 2009 (Birdlife International, 2017).

741 Ongoing changes in populations of penguins may also reflect the impact of
742 changing sea surface temperatures. Higher sea surface temperatures have already
743 reduced sea ice, leading to a reduction in Antarctic krill, a vital food source for
744 penguins in the Antarctic region (Brierly, 2008). Failure in krill recruitment may
745 lead to a decline in penguin populations (Trathan et al., 2007). Adelie penguin
746 populations have decreased over the past 25 years because of a reduction in their
747 food supply (Forcada et al., 2006). However, with the climate becoming milder
748 at these latitudes, the environment is more suited to Gentoo penguins (*Pygoscelis*
749 *papua*), which have increased in numbers (Forcada et al., 2006). These examples
750 illustrate the complexity of forecasting overall changes in NH₃ emissions in future
751 scenarios, if both the direct and indirect effects of climate change on bird
752 populations are taken into account in a model system.

753 It is clear, however, that changes in seabird populations will result in changes to the
754 nitrogen dynamics of the surrounding ecosystems. This especially true for
755 environments where naturally occurring nutrients are scarce, such as in sub-polar
756 or arid tropical climates, where small changes to the amount of seabird-mediated
757 marine nutrients imported to terrestrial ecosystems could result in substantial
758 changes to plant productivity.

759 **4. Conclusions**

760 This paper has presented the results of simulations using the process based GUANO
761 model to further our understanding of global NH₃ emissions from seabird colonies
762 and how these may alter under climate change. The results present the first global
763 maps of NH₃ emissions from seabird colonies using a dynamic model driven by
764 meteorological conditions. The meteorology driven model of NH₃ emissions allow
765 future scenarios to be predicted of the climate change effect on ammonia emissions
766 from seabirds, expressed both as total NH₃ emission and as a percentage
767 volatilization of the excreted nitrogen (P_v). According to IPCC Scenarios A2, A1B
768 and B2, we estimate annual NH₃ emissions for 2099 of 114, 112 and 104 Gg yr⁻¹,
769 respectively. Although emissions are predicted to decrease at a few locations,
770 where increased precipitation is estimated to outweigh the effect of warmer
771 conditions in increasing emission, overall the global picture is that climate change
772 will tend to increase global ammonia emissions from seabirds by around 20 to 40%,
773 depending on the climate scenario for 2099.

774 The present study provides a first application of how a process model of ammonia
775 emissions from animals, accounting for diurnal and seasonal dynamics, can be

776 applied at a global scale. In so doing it simultaneously provides a demonstration of
777 how the approach can be used to assess scenarios of future climate change and
778 illustrates the potential of the GUANO model for broader application for other
779 livestock NH₃ emission sources at the global scale.

780 **Acknowledgments**

781 The work described in this paper was supported by grants from the NERC CEH
782 Environmental Change Integrating Fund (ECIF), the NERC thematic programme
783 (GANE) and ongoing NERC National Capability programme. It provides modelling
784 underpinning as a contribution to Activity 1.5 of the International Nitrogen
785 Management System (and the '*Towards INMS*' project), under the overall lead of
786 UN Environment and the International Nitrogen Initiative (INI). Thanks to D.
787 Briggs of British Antarctic Survey (BAS) on Signy for information on meteorology
788 and nesting penguins, and the BAS Bird Island crew for their technical and physical
789 support (BAS CGS grant). Thanks to the CEH coastal seas ecology group and other
790 researchers on the Isle of May, especially to M. A. Newell, M. P. Harris (both CEH),
791 T. Alampo and D. Pickett (both Scottish National Heritage). We are grateful to L.
792 J. Wilson (CEH) for initial work on the seabird database and seabird NH₃ emissions
793 and all contributors that provided data for the seabird database: Birdlife
794 International, E. Woehler (University of Tasmania, Australia), H. Strom (Nordic
795 Seabird Group), Y. Yu (Hong Kong Bird Society), R. Mavor (JNCC, UK), D. Irons
796 (US FWS), Canada's Important Bird Areas, Australian Department for
797 Environment, G. Taylor (Department of Conservation, NZ), P. Yorio (Centro
798 Nacional Patagónico), C. A. Yeap (Malaysian Nature Society), P. Round (Mahidol
799 University), A. Petersen (Icelandic Institute of Natural History), C. Egevang
800 (Greenland Institute of Natural Resources), T. Yamamoto (Japan National Institute
801 of Polar Research), T. Anker-Nilssen (Norwegian Institute for Nature Research), J.
802 Elts (Estonian Ornithological Society), M. Hario (Finnish Game and Fisheries
803 Research), Y. Artukhin (Pacific Institute of Geography), M. Paleczny (UBC), R.
804 Allen (Florida Fish and Wildlife Conservation Commission), C. Kisiel (NJ Fish and
805 Wildlife, USA), M. Gibbons, D. Rosenblatt (both Stony Brook University), S.
806 Cameron (North Carolina Wildlife Resources Commission), B. Ortego (US FWS
807 Texas), S. Stephensen (US FWS Oregon) and R. Boettcher (VA Game and Inland
808 Fisheries).

809 **References**

- 810 Anderson, W. B. and Polis, G. A. (1999) Nutrient fluxes from water to land:
811 seabirds affect plant nutrient status on Gulf of California islands. *Oecologia*, 118,
812 324-332.
- 813 Bash, J. O., Cooter, E. J., Dennis, R. L., Walker, J. T. and Pleim, J. E.
814 (2012) Evaluation of a regional air-quality model with bi-directional NH₃ exchange
815 coupled to an agro-ecosystem model. *Biogeosciences* 10, 1635–1645. doi:10.5194/bg-
816 10-1635-2013
- 817 Birdlife International (2017) Accessed June 2017. URL was correct at a given date.
818 <http://datazone.birdlife.org/home>.
- 819 Blackall, T. D., Wilson, L. J., Bull, J., Theobald, M. R., Bacon, P. J., Hamer, K. C.,
820 Wanless, S. and Sutton, M. A. (2008) Temporal variation in atmospheric ammonia
821 concentrations above seabird colonies. *Atmospheric Environment*, 42, 6942-6950.

- 822 Blackall, T. D., Wilson, L. J., Theobald, M. R., Milford, C., Nemitz, E., Bull, J.,
823 Bacon, P. J., Hamer, K. C., Wanless, S. and Sutton, M. A. (2007) Ammonia
824 emissions from seabird colonies. *Geophysical Research Letters*, 34, 5-17.
- 825 Brierley, A. S. (2008) Antarctic Ecosystem: Are deep krill ecological outliers or
826 portents of a paradigm shift? *Current Biology*, 18, 252-254.
- 827 Croft, B., Wentworth, G. R., Martin, R. V., Leitch, W. R., Murphy, J. G., Murphy,
828 B. N., Kodros, J. K., Abbatt, J. P. D., and Pierce, J. R.: Contribution of Arctic
829 seabird-colony ammonia to atmospheric particles and cloud-albedo radiative effect,
830 *Nat. Comm.*, 7, 13444, 2016.
- 831 EC-JRC/PBL (2010) Emission Database for Global Atmospheric Research
832 (EDGAR), release version 4.1. Accessed January 2017., European Commission,
833 Joint Research Centre (JRC) / Netherlands Environmental Assessment Agency
834 (PBL). <http://edgar.jrc.ec.europa.eu>.
- 835 Egevang, C., Stenhouse, I. J., Phillips, R. A., Petersen, A., Fox, J. W. and Silk, J.
836 R. D. (2010) Tracking of Arctic terns *Sterna paradisaea* reveals longest animal
837 migration. *Proceedings of the National Academy of Sciences of the United States*
838 *of America*, 107, 2078-2081.
- 839 Elliott, H. A. & Collins, N. E. (1982) Factors affecting ammonia release in broiler
840 houses. *Transactions of the ASAE*, 25, 413.
- 841 Ellis, J. C. (2005) Marine birds on land: a review of plant biomass, species richness,
842 and community composition in seabird colonies. *Plant Ecology*, 181, 227-241.
- 843 Forcada, J., Trathan, P. N., Reid, K., Murphy, E. J. and Croxall, J. P. (2006)
844 Contrasting population changes in sympatric penguin species in association with
845 climate warming. *Global Change Biology*, 12, 411-423.
- 846 Fretwell, P. T., Scofield, P. and Phillips, R. A. (2017), Using super-high resolution
847 satellite imagery to census threatened albatrosses. *Ibis*, 159: 481-490.
848 doi:10.1111/ibi.12482.
- 849 Gu, B., Sutton, M. A., Chang, S. X., Ge, Y., and Chang, J.: Agricultural ammonia
850 emissions contribute to China's urban air pollution, *Front. Ecol. Environ.*, 12, 265-
851 266, doi:10.1890/14.WB.007, 2014.
- 852 IPCC (2007) Intergovernmental Panel on Climate Change 2007, The Physical
853 Science Basis. Contribution of Working Group I to the Fourth Assessment Report
854 of the IPCC.
- 855 IPCC (2013) Climate Change 2013: The Physical Science Basis. In: Stocker, T.F.,
856 Qin, D., Plattner, G.-K., Tignor, M., Allen, S.K., Boschung, J., Nauels, A., Xia, Y.,
857 Bex, V., Midgley, P.M. (Eds.), Contribution of Working Group I to the Fifth
858 Assessment Report of the Intergovernmental Panel on Climate Change. Cambridge
859 University Press, Cambridge, United Kingdom and New York, NY, USA, p. 1535.
860 <http://dx.doi.org/10.1017/CBO9781107415324>.
- 861 IPCC Data (2017) Intergovernmental Panel on Climate Change - Data Distribution
862 Center. Accessed January 2017 URL was correct at a given date. <http://www.ipcc->
863 [data.org/](http://www.ipcc-data.org/).

864 Lindeboom, H. J. (1984) The nitrogen pathway in a penguin rookery. *Ecology*, 65,
865 269-277.

866 Mann, M. E. and Kump, L. R. (2008) *Dire predictions: understanding global*
867 *warming*, DK Publishing.

868 Móríng A., Vieno M., Doherty R.M., Laubach J., Taghizadeh-Toosi A. and Sutton
869 M.A. (2016) A process-based model for ammonia emission from urine patches,
870 GAG (Generation of Ammonia from Grazing): description and sensitivity analysis.
871 *Biogeosciences* 13, 1837-1861.

872 NCDC (2011) National Climatic Data Center, Integrated Surface Hourly (ISH)
873 database. <https://www.ncdc.noaa.gov/data-access>. Accessed January 2017. URL
874 was correct at a given date.

875 NCEP (2011) National Centres for Environmental Protection / National Center for
876 Atmospheric Research NCEP/NCAR Reanalysis project. Accessed January 2017.
877 URL was correct at a given date.
878 <http://www.esrl.noaa.gov/psd/data/reanalysis/reanalysis.shtml>.

879 Nemitz, E., Milford, C. and Sutton, M. A. (2001) A two-layer canopy compensation
880 point model for describing bi-directional biosphere-atmosphere exchange of
881 ammonia. *Quarterly Journal of the Royal Meteorological Society*, 127, 815-833.

882 Parton, W. J. and Logan, J. A. (1981) A model for diurnal variation in soil and air
883 temperature. *Agricultural and Forest Meteorology*, 23, 205-216.

884 Riddick, S., Dragosits, U., Blackall, T., Daunt, F., Wanless, S., and Sutton, M. A.
885 (2012) Global ammonia emissions from seabird, *Atmos. Environ.*, 55, 312-327.

886 Riddick S., Dragosits U., Blackall T., Daunt F., Braban, C. F., Tang, Y. S.,
887 MacFarlane, W., Taylor, S., Wanless S. and Sutton M.A. (2014) Measurement of
888 ammonia emissions from tropical seabird colonies. *Measurement of ammonia*
889 *emissions from tropical seabird colonies. Atmospheric Environment* 89. 35-42.

890 Riddick S., Dragosits U., Blackall T., Daunt F., Newell, M., Braban, C. F., Tang,
891 Y. S., Schmale, J., Hill, P., Wanless, S., Trathan, P. and Sutton M.A. (2016a)
892 Measurement of ammonia emissions from temperate and polar seabird colonies.
893 *Atmospheric Environment* 134, 40-50.

894 Riddick, S., Hess, P., Mahowald, N. and Ward, D.S. (2016a) The modeled response
895 of terrestrial nitrogen pathways to changes in agricultural nitrogen from 1850 to the
896 present using the CESM. Estimate of changes in agricultural terrestrial nitrogen
897 pathways and ammonia emissions from 1850 to present in the Community Earth
898 System Model, *Biogeosciences* 13, 3397-3426.

899 Riddick, S. N., Blackall, T. D., Dragosits, U., Tang, Y. S., Moring, A., Daunt, F.,
900 Wanless, S., Hamer, K. C., and Sutton, M. A. (2017) High temporal resolution
901 modelling of environmentally-dependent seabird ammonia emissions: Description
902 and testing of the GUANO model, *Atmos. Environ.*, 161, 48-60.

903 Riedo, M., Milford, C., Schmid, M. and Sutton, M.A. (2002) Coupling soil-plant-
904 atmosphere exchange of ammonia with ecosystem functioning in grasslands.
905 *Ecological Modelling* 158, 83-110.

- 906 Santander, H. (1981) Patterns of distribution and spawning fluctuations of anchovy
907 and sardines. *Boletín del Instituto del Mar de Perú*, Vol. extraordinario, 180-192.
- 908 Speir, T. W., and Ross, D. J. (1984) Ornithogenic Soils of the Cape Bird Adélie
909 Penguin Rookeries, Antarctica 2. *Ammonia Evolution and Enzyme Activities*, *Polar*
910 *Biol.*, 2, 207-212.
- 911 Stulen, I., Perez-Soba, M., De Kok, L. J. and Van Der Eerden, L. (1998) Impact of
912 gaseous nitrogen deposition on plant functioning. *New Phytologist*, 139, 61-70.
- 913 Sutton, M. A., Erisman J. W., Dentener F. & Möller D. (2008) Ammonia in the
914 environment: From ancient times to the present. *Environmental Pollution*, 156, 583-
915 604.
- 916 Sutton, M. A., Howard, C. M. and Erisman, J. W. (Eds.) (2011) *The European*
917 *Nitrogen Assessment: Sources, Effects and Policy Perspectives*, Cambridge
918 University Press.
- 919 Sutton M.A., Reis R., Riddick S.N., Dragosits U., Nemitz E., Theobald M.R., Tang
920 Y.S., Braban C.F., Vieno M., Dore A.J., Mitchell R.F., Wanless S., Daunt F.,
921 Fowler D., Blackall T.D., Milford C., Flechard C.F., Loubet B., Massad R., Cellier
922 P., Coheur P.F., Clarisse L., van Damme M., Ngadi, Y., Clerbaux C., Skjøth C.A.,
923 Geels C., Hertel O., Wichink Kruit R.J., Pinder, R.W., Bash J.O., Walker J.D.,
924 Simpson D., Horvath, L., Misselbrook, T.H., Bleeker A., Dentener F. & Wim de
925 Vries V. (2013) Toward a climate-dependent paradigm of ammonia emission &
926 deposition. *Phil. Trans. Roy. Soc. (Ser. B)*. 368: 20130166.
927 <http://dx.doi.org/10.1098/rstb.2013.0166>
- 928 Trathan, P. N., Forcada, J. and Murphy, E. J. (2007) Environmental forcing and
929 Southern Ocean marine predator populations: effects of climate change and
930 variability. *Philosophical Transactions of the Royal Society B-Biological Sciences*,
931 362, 2351-2365.
- 932 Weber, R. J., McMurry, P. H., Mauldin, L., Tanner, D. J., Eisele, F. L., Brechtel, F.
933 J., Kreidenweis, S. M., Kok, G. L., Schillawski, R. D., and Baumgardner, D.: A
934 study of new particle formation and growth involving biogenic and trace gas species
935 measured during ACE 1, *J. Geophys. Res.-Atmos.*, 103, 16385-16396, 1998.
- 936 Wilson, L. J., Bacon, P. J., Bull, J., Dragosits, U., Blackall, T. D., Dunn, T. E.,
937 Hamer, K. C., Sutton, M. A. and Wanless, S. (2004) Modelling the spatial
938 distribution of ammonia emissions from seabirds in the UK. *Environmental*
939 *Pollution*, 131, 173-185.
- 940 Wyrski, K. (1975) El-Niño - Dynamic response of equatorial Pacific Ocean to
941 atmospheric forcing. *Journal of Physical Oceanography*, 5, 572-584.
- 942 Zhu, R., Sun, J., Liu, Y., Gong, Z. and Sun, L. (2011) Potential ammonia emissions
943 from penguin guano, ornithogenic soils and seal colony soils in coastal Antarctica:
944 effects of freezing-thawing cycles and selected environmental variables. *Antarctic*
945 *Science*, 23, 78-92.
- 946

947 **Table 1 Comparison of global NH₃ emission from seabirds in 2099 to IPCC climate change scenarios**
 948 **B1, A1B and A2.**

| | 2010 | B1 2099 | A1B 2099 | A2 2099 |
|---|--------------------|---------------------|---------------------|---------------------|
| Total NH ₃ emission [uncertainty range] (Gg NH ₃ year ⁻¹) | 81.8 [37 - 127] | 103.7 [48 – 160] | 111.6 [51 – 172] | 113.8 [52 – 175] |
| Change from 2010 emission estimate (%) | | +26.8 | +36.4 | +39.1 |

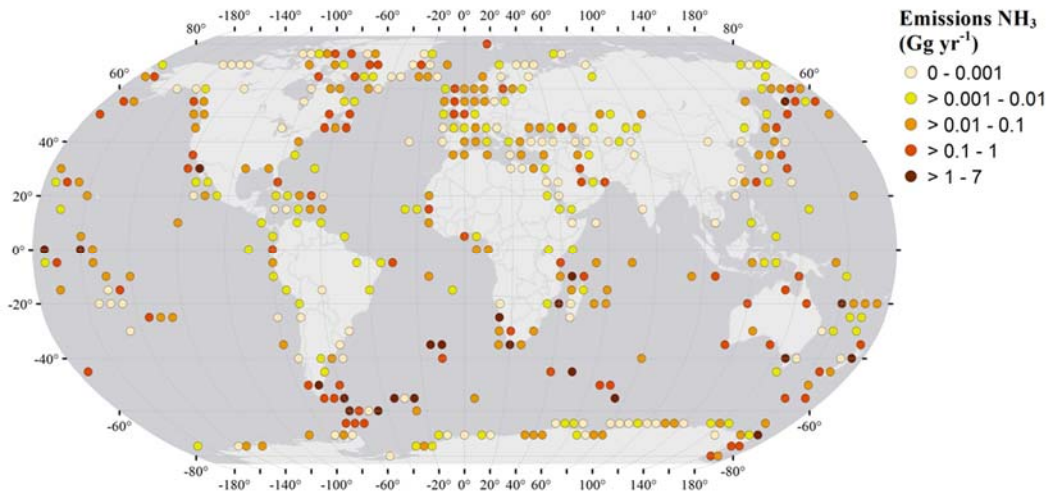
949

950 **Table 2 Average percentage of nitrogen that volatilizes (P_v) for a range of species. With temperature (T)**
 951 **in 2099 (IPCC Scenario A2) and P_v for 2010 (IPCC Scenario A2).**

| Species | Average T during breeding 2010 (°C) | Average P_v 2010 (%) | Average T during breeding 2099 (°C) | Average P_v 2099 (%) | Change in average P_v 2010 to 2099 (%) |
|--------------------------------|--|------------------------------|--|------------------------------|---|
| Emperor Penguin ^{1,5} | -15.9 | 0.4 | -14.4 | 0.6 | +0.2 |
| Snowy Sheathbill | -2.6 | 2.2 | -1.3 | 2.1 | -0.1 |
| Adelie Penguin | -10.2 | 2.7 | -8.9 | 3.3 | +0.6 |
| Atlantic Puffin | 9.1 | 3.1 | 11.8 | 7.7 | +4.7 |
| Macaroni Penguin | 1.1 | 4.4 | 2.5 | 3.2 | -1.2 |
| Brown Noddy | 27.1 | 25.8 | 32.6 | 47.4 | +21.6 |
| Sooty Tern | 27.1 | 40.7 | 32.6 | 60.6 | +20.1 |
| Little Black Shag ³ | 13.3 | 10.3 | 17.5 | 60.0 | +49.7 |
| Peruvian Booby ⁶ | 20.0 | 65.9 | 23.6 | 72.3 | 6.4 |
| Peruvian Tern ^{2,4} | 21.0 | 68.0 | 25.1 | 62.0 | -6.0 |

952 Notes: ¹Smallest estimated P_v value for a seabird species in 2010. ²Largest estimated P_v value for a
 953 seabird species in 2010. ³Largest simulated climate change driven increase for a seabird species. ⁴
 954 Largest simulated climate change driven decrease for a seabird species. ⁵Smallest estimated P_v value
 955 for a seabird species in 2099. ⁶Largest estimated P_v value for a seabird species in 2099.

956

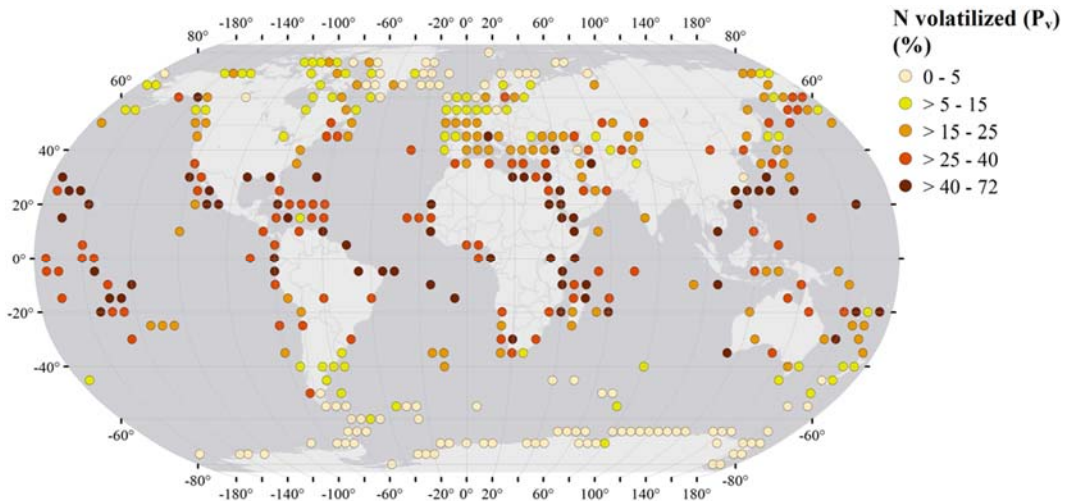


957

958

959

Figure 1 Global NH_3 emissions from seabirds aggregated for each 5 degree square, calculated using the GUANO model with ground temperature data, for 2010 (baseline).



960

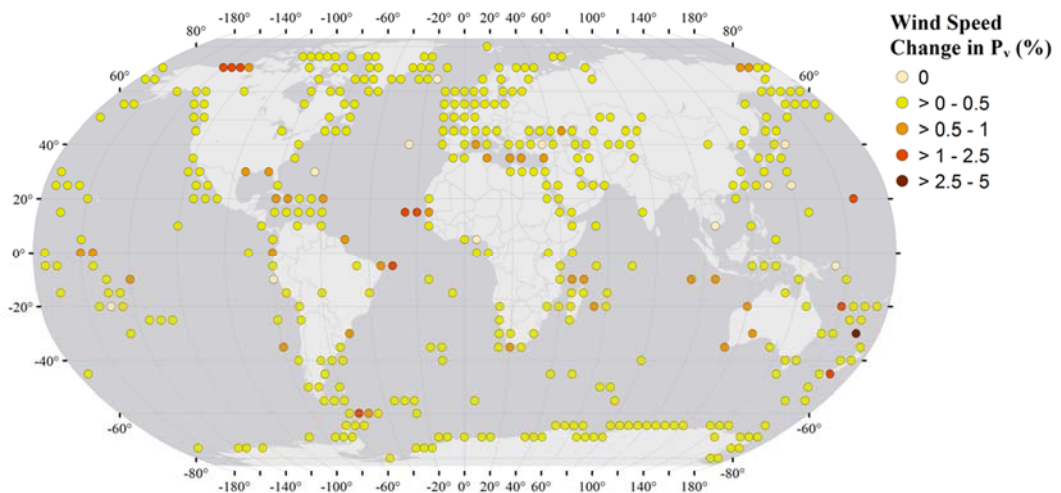
961

962

Figure 2 Spatial distribution of the percentage of excreted nitrogen that volatilizes (P_v) at seabird colonies, calculated using the GUANO model for 2010 (baseline).

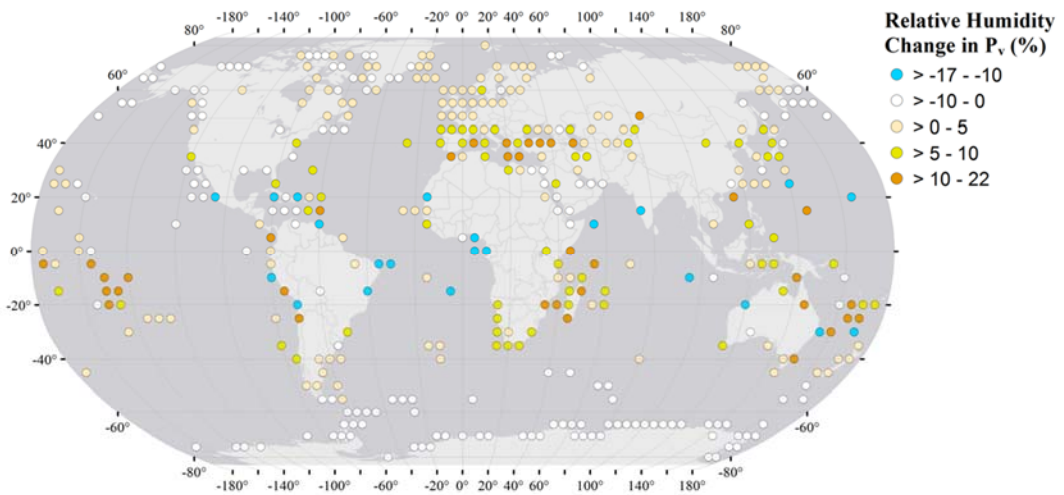
963

a)



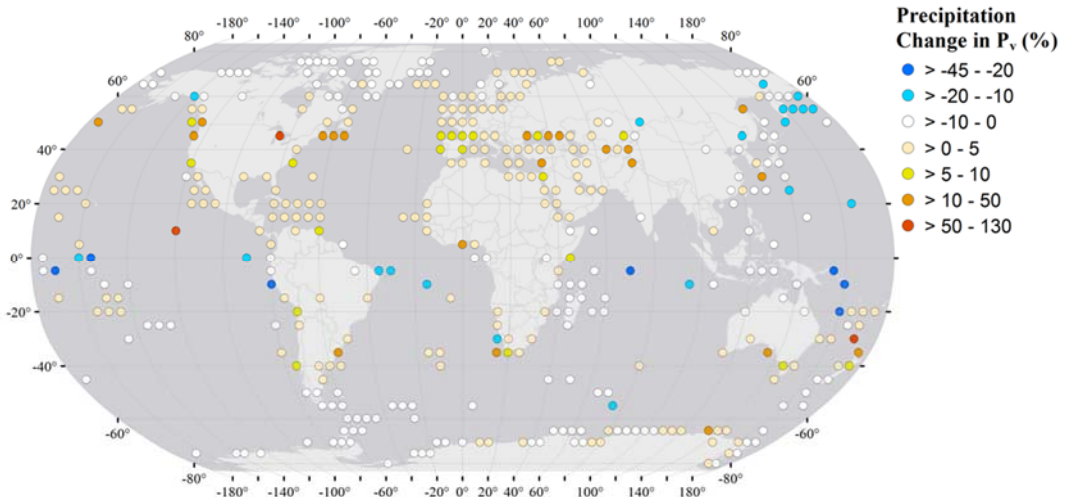
964

965 b)



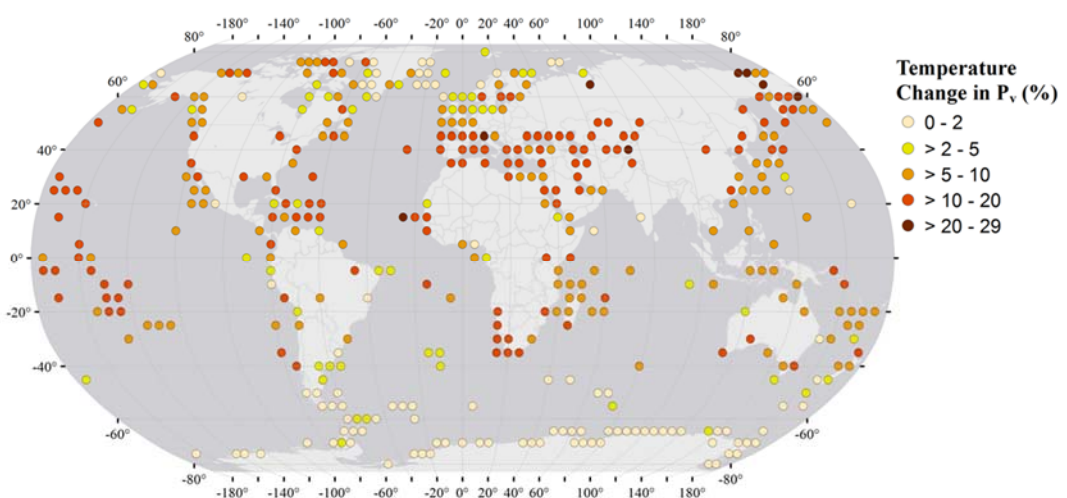
966

967 c)



968

969 d)



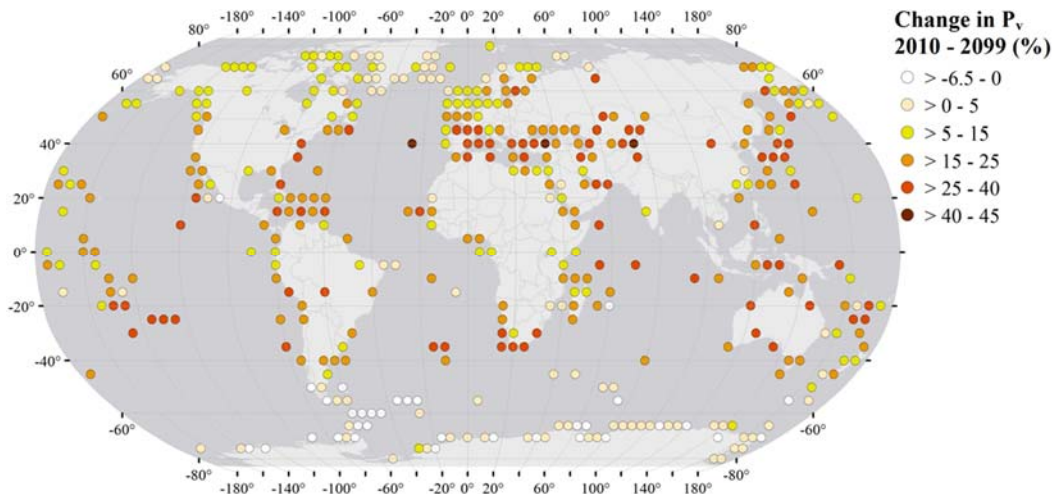
970

971

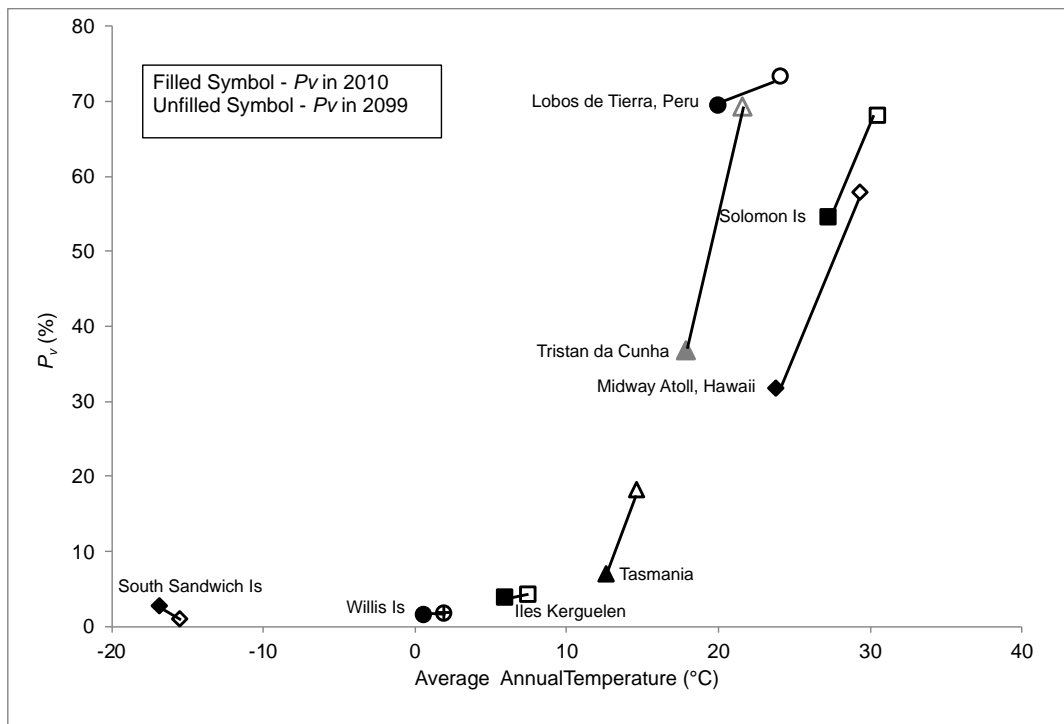
972

Figure 3 Changes to percentage of excreted nitrogen that volatilizes (P_v) estimated between 2010 and 2009 at seabird colonies when a) wind speed anomalies are considered only, b) relative humidity

973 anomalies are considered only, c) precipitation anomalies are considered only and d) temperature
 974 anomalies are considered only. Climate anomalies are taken from the IPCC A2 climate change scenario
 975 (IPCC DDC, 2011).
 976



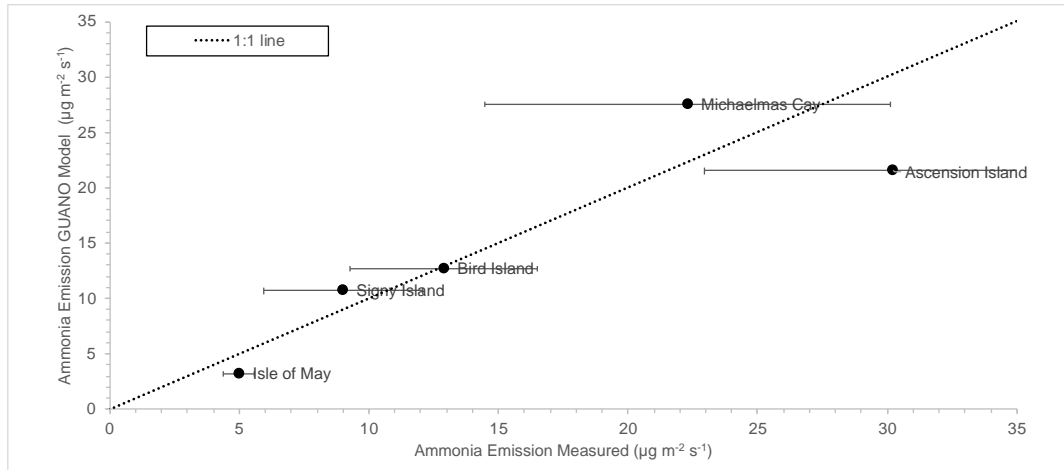
977
 978 **Figure 4** Changes to percentage of excreted nitrogen that volatilizes (P_v) estimated for 2099 at seabird
 979 colonies when all climate anomalies are considered, using the IPCC A2 Scenario.



980
 981 **Figure 5** Effects of climate change on P_v at the 8 largest seabird colonies, calculated with the GUANO
 982 model. Filled symbols indicate NH_3 emissions for 2010 using Global Summary of Day (GSOD); unfilled
 983 symbols represent predicted NH_3 emissions by incorporating temperature, wind speed, relative humidity
 984 and precipitation anomalies for 2099 (IPCC Scenario A2).
 985

986

A

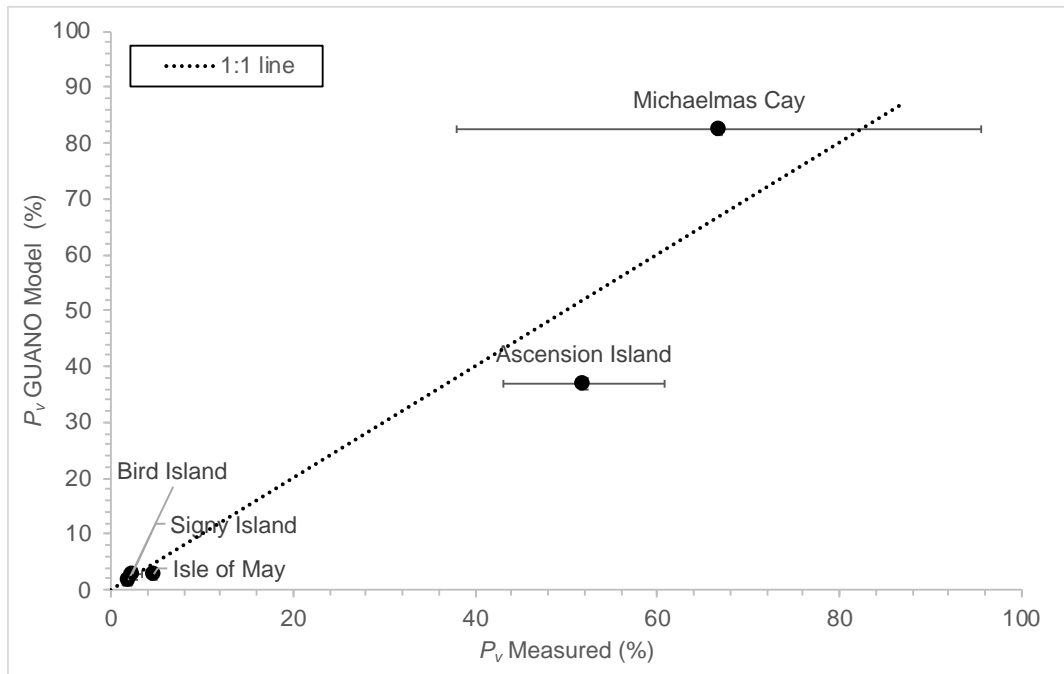


987

988

B

989



990

991

992

993

994

995

996

997

998

999

Figure 6 Comparison of (a) the area-based NH_3 emission value and (b) the P_v value calculated by the GUANO model with micrometeorological measured data for site based measurements. Values refer to the periods of the measurements used. For further details see Riddick et al. (2014; 2016a; 2017). Sites: Sooty terns on rocks, Ascension Island (Mid Atlantic); Puffin burrow area with grass, Isle of May (Scotland); Macaroni penguins on rock, Bird Island (South Georgia, South Atlantic); Common noddys on bare ground, Michaelmas Cay (Northern Australia); Chinstrap penguins on bare rock, Signy Island (South Atlantic). Description of the uncertainty analysis used to calculate the error bars presented are found in Riddick et al. (2014; 2016a).

1000 **Supplementary Material Section 1: A comparison of the diurnal air**
 1001 **temperatures derived from Parton and Logan (1981) with measured values**

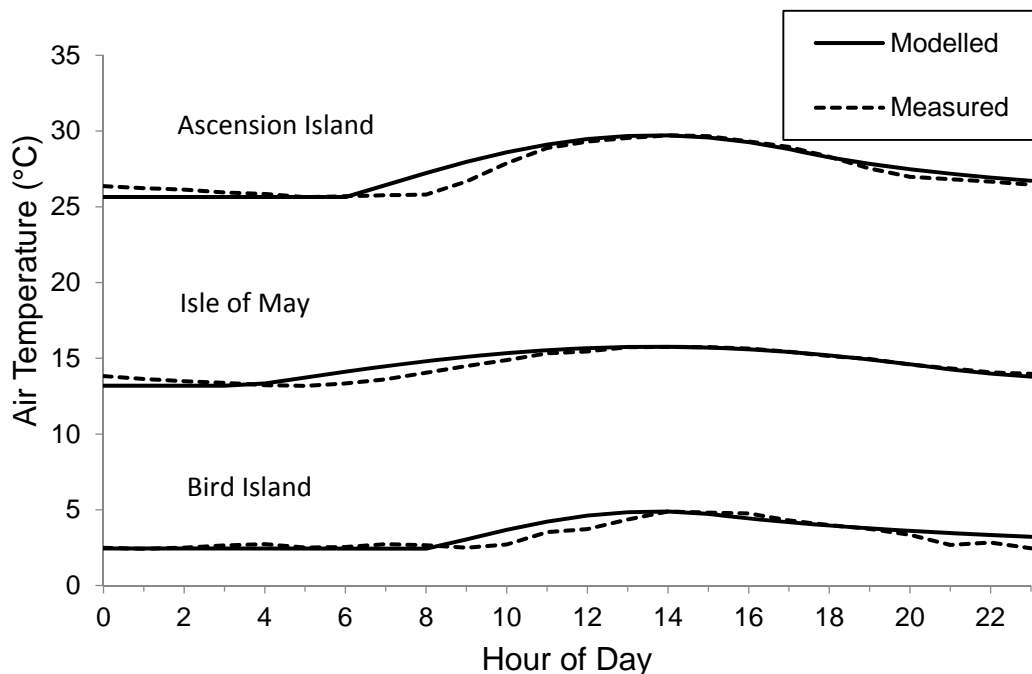
1002 Figure SM1.1 shows the diurnal variation in air temperature according to the Parton
 1003 and Logan (1981) model plotted against the measured air temperature data at 2 m
 1004 above ground level for Ascension Island, the Isle of May and Bird Island. A linear
 1005 regression shows good agreement between the modelled and measured values for
 1006 the field sites. The coefficient of determination for each site is shown in Table
 1007 SM1.1.

1008 **Table SM1.1 Comparison between average measured ground temperature and ground temperatures**
 1009 **modelled with the Parton and Logan (1982) method, using measured average maximum and minimum**
 1010 **air temperature data during the measurement period at each of the field sites.**

| Field site | Slope | R ² |
|----------------------|-------|----------------|
| Isle of May | 0.90 | 0.89 |
| Mars Bay, Ascension | 0.88 | 0.84 |
| Big Mac, Bird Island | 0.84 | 0.79 |

1011

1012 Although the temperatures calculated by the Parton and Logan (1981) model are
 1013 serially correlated, the model describes the hourly values of the temperature well in
 1014 temperate, tropical and polar regions during the seabird breeding season (Figure
 1015 SM1.1). However, it should be noted that the Parton and Logan (1981) model
 1016 overestimates temperatures as the temperature increases (dawn) and as it decreases
 1017 (dusk).



1018
 1019
 1020
 1021

Figure SM1.1 Comparison of the diurnal variation in average measured ground temperature and ground temperatures modelled with the Parton and Logan (1982) method, using measured average maximum and minimum air temperature data during the measurement period at each of the field sites.

1022 **Supplementary Material Section 2: Comparison of data from the National**
 1023 **Climatic Data Center (NCDC) and Global Surface Summary of the Day**
 1024 **(GSOD) data (NCDC, 2011) to the data observed during the measurement**
 1025 **campaign of Riddick et al. (2014; 2016a)**

1026 To determine the most suitable meteorological dataset for use in the global GUANO
 1027 model, the detailed meteorological data measured from each field work site were
 1028 compared with two available global meteorological datasets:

- 1029 • National Climatic Data Center (NCDC) Global Surface Summary of the
 1030 Day (GSOD) data (NCDC, 2011) and
- 1031 • The National Center for Environmental Prediction and the National Center
 1032 for Atmospheric Research (NCEP/NCAR) reanalysis data set (NCEP,
 1033 2011).

1034 The NCDC GSOD data were available as daily data (Integrated Surface Hourly
 1035 (ISH) dataset), collated by the USAF Climatology Center. The dataset includes
 1036 observed data from over 9000 meteorological stations globally. A minimum of four
 1037 observations is used to derive the daily summary data. Due to unit conversions to
 1038 the metric system, slight rounding errors may occur. Data reports are based on
 1039 Greenwich Mean Time (GMT). The available data are summarised in Table SM2.1
 1040 below:

1041 **Table SM2.1 Summary of data available from the National Climatic Data Center (NCDC) Global**
 1042 **Surface Summary of the Day (GSOD) (NCDC, 2011)**

| Variable | Unit | Accuracy |
|------------------------------|------------|----------|
| Mean temperature | Fahrenheit | 0.1 |
| Mean dew point | Fahrenheit | 0.1 |
| Mean visibility | Miles | 0.1 |
| Mean Wind Speed | Knots | 0.1 |
| Maximum sustained wind speed | Knots | 0.1 |
| Maximum wind gust | Knots | 0.1 |
| Maximum temperature | Fahrenheit | 0.1 |
| Minimum temperature | Fahrenheit | 0.1 |
| Precipitation amount | Inches | 0.01 |
| Snow depth | Inches | 0.1 |

1043

1044 The NCEP/NCAR data are derived using an analysis/forecast system, which uses
 1045 weather observations taken by ships, planes, station data and satellite observations.
 1046 The data are available in 4-times daily (i.e., 6-hourly) format or as daily averages
 1047 at a 2.5 ° x 2.5 ° grid resolution, and include air temperature at the surface (°C),
 1048 relative humidity (%), precipitation rate (kg m⁻² s⁻¹), wind speed (m s⁻¹), net solar

1049 radiation ($W m^{-2}$) and ground temperature ($^{\circ}C$). The largest uncertainty is
 1050 associated with the air temperature at the surface (or “skin temperature”), which is
 1051 determined diagnostically as the temperature to balance the fluxes at the surface.
 1052 The method used to calculate the skin temperature is acknowledged to fail in
 1053 conditions with low wind speeds and when the thermal exchange coefficient is close
 1054 to zero (NCEP, 2011). The net solar radiation data are empirically based and take
 1055 into account cloud cover.

1056 To evaluate the two global datasets for their suitability for estimating global
 1057 ammonia emissions, meteorological data for the field sites on Ascension, the Isle of
 1058 May and Bird Island were obtained from both the GSOD and NCEP/NCAR datasets
 1059 and compared with measured data collected during the field work carried out for
 1060 this thesis. The NCEP/NCAR data were taken from the grid cell that contained the
 1061 bird colony, whereas the GSOD data were taken from the meteorological station
 1062 geographically closest to the bird colony (Table SM2.2).

1063 **Table SM2.2 The name and distance of the GSOD meteorological station geographically closest to the**
 1064 **bird colony.**

| Field site | Met station name (NCDC ID #) | Distance between field site and met station (km) |
|----------------------|--|--|
| Isle of May | Leuchars Airbase, Fife (31710) | 30 |
| Mars Bay, Ascension | Wideawake airhead, Ascension Island (619020) | 1 |
| Big Mac, Bird Island | Base Orcadas, Laurie Island, South Orkney Islands (889680) | 850 |

1065

1066 Hourly values of air temperature, relative humidity, wind speed and precipitation
 1067 were calculated from the GSOD data. Hourly air temperature was calculated using
 1068 daily maximum and minimum values using the Parton and Logan (1982) method.
 1069 Hourly values of relative humidity data were taken as the daily average, as were the
 1070 values for wind speed. The hourly value of precipitation was simply the total daily
 1071 value divided by 24.

1072 To make a direct comparison between the data sets, hourly values of NCEP/NCAR
 1073 meteorological data were calculated in the same way as for the GSOD data. The
 1074 NCEP/NCAR dataset also included ground temperature and net solar radiation data.
 1075 Hourly ground temperatures were calculated the same way as hourly air
 1076 temperatures, using the Parton and Logan (1982) model. Net solar radiation during
 1077 the hours of night was set at zero, where the hours of night were calculated using
 1078 the method of Parton and Logan (1982). The hourly solar radiation during the day
 1079 was calculated as the daily average value during the hours of daylight.

1080 To identify which dataset best represents the actual meteorology at the colony, the
 1081 two sets of hourly data (GSOD and NCEP/NCAR) were compared with the hourly
 1082 values of meteorological data measured in this study at the three field sites. The
 1083 quality of fit is determined by calculating the gradient (m) and coefficient of

1084 determination (R^2) of the linear regression between measured and GSOD or
 1085 NCEP/NCAR values, respectively, for each meteorological variable.

1086 GSOD data accord more closely to meteorological data measured at Bird Island, the
 1087 Isle of May and Ascension Island than NCEP/NCAR data (Tables SM2.3; SM2.4).
 1088 However, the fit of the GSOD data depends on the proximity of the meteorological
 1089 station to the seabird colony and also the local conditions (e.g., influence of
 1090 topography on wind speed/direction). These issues are particularly noticeable by
 1091 the poor correlation between the GSOD meteorological data measured at Base
 1092 Orcadas and those measured on Bird Island in the field ($R^2 = 0.10 - 0.13$), which
 1093 may be caused by the distance between Base Orcadas and Bird Island (850 km).
 1094 Despite these differences, the GSOD data are still a better fit to measured data than
 1095 the NCEP data. The GSOD and NCEP/NCAR precipitation both agree well with
 1096 measured precipitation data, but the GSOD agrees better with the higher
 1097 precipitation measured on the Isle of May. The GSOD data for air temperature,
 1098 relative humidity, wind speed and precipitation are the best available
 1099 meteorological data, while the NCEP/NCAR provides the best net solar radiation
 1100 data available. The NCEP/NCAR ground temperature data do not fit well to
 1101 measured values. The poor fit is due to the large area covered by the $2.5^\circ \times 2.5^\circ$
 1102 grid cells. Each of the three islands occupies only a very small proportion of the
 1103 respective grid cell, thus the data is more representative of the sea surface
 1104 temperature rather than the land surface temperature of the grid cell. Therefore, the
 1105 NCEP/NCAR ground temperature data are not suitable for use in the emission
 1106 model.

1107 **Table SM2.3 Comparison of measured data to Global Summary Of Day (GSOD) data with data**
 1108 **measured at the field sites, for the duration of the field work. T_A is air temperature, RH is the relative**
 1109 **humidity, WS is wind speed and P is the total precipitation measured during the period of field work.**
 1110 **The gradient of the linear regression is denoted as m and R^2 is the coefficient of determination between**
 1111 **the measurements and the GSOD database.**

| | Hourly T_A | | Hourly RH | | Hourly WS | | Total P | |
|-------------|--------------|------|-----------|------|-----------|------|------------------|--------------|
| | R^2 | m | R^2 | m | R^2 | m | Measured (mm) | GSOD (mm) |
| Isle of May | 0.57 | 1.3 | 0.58 | 0.81 | 0.40 | 0.35 | 110 | 76 |
| Ascension | 0.64 | 0.80 | 0.20 | 0.50 | 0.10 | 0.19 | 6 | 11 |
| Bird Island | 0.10 | 0.25 | 0.10 | 0.22 | 0.13 | 0.20 | 98 | 76 |

1112

1113

1114 **Table SM2.4 Comparison of measured data for the duration of the field work to National Center for**
 1115 **Environmental Prediction and the National Center for Atmospheric Research (NCEP/NCAR) data. T_A**
 1116 **is air temperature, T_G is ground temperature, RH is the relative humidity, WS is wind speed, R_n is net**
 1117 **radiation and P is precipitation. The gradient of the linear regression is denoted as m and R^2 is the**
 1118 **coefficient of determination between the measurements and the NCEP/NCAR database.**

| | Hourly T_A | | Hourly T_G | | Hourly RH | | Hourly WS | | Hourly I_r | | Total P |
|-------------|--------------|------|--------------|------|-----------|------|-----------|------|--------------|------|-----------------------|
| | R^2 | m | R^2 | m | R^2 | m | R^2 | m | R^2 | m | NCEP/ NCAR (mm) |
| Isle of May | 0.50 | 0.64 | 0.01 | 0.02 | 0.12 | 0.47 | 0.30 | 0.32 | 0.45 | 0.56 | 62 |

| | | | | | | | | | | | |
|-------------|------|------|------|------|------|------|------|------|------|------|----|
| Ascension | 0.06 | 0.12 | 0.01 | 0.01 | 0.02 | 0.05 | 0.02 | 0.18 | 0.52 | 0.60 | 12 |
| Bird Island | 0.03 | 0.17 | 0.01 | 0.02 | 0.18 | 0.02 | 0.03 | 0.01 | 0.34 | 0.40 | 79 |

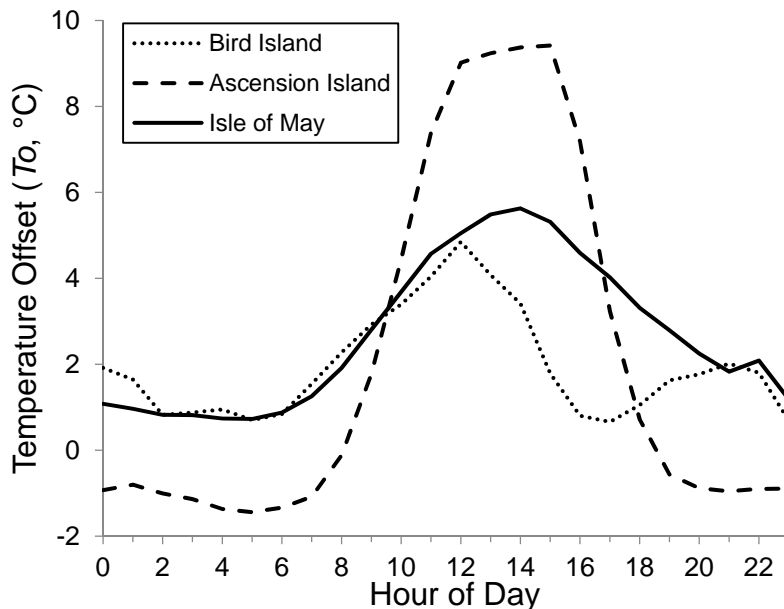
1119

1120

1121 **Supplementary Material Section 3: Calculating the temperature offset (T_o)**
1122 **function from air temperature data and surface temperature data from the**
1123 **three field work sites measured during the campaigns of Riddick et al. (2014,**
1124 **2016a)**

1125 Ground temperature is different from air temperature measured at 2 m and has a
1126 large influence on NH_3 emission calculations in the GUANO model. Ground
1127 temperature is very rarely measured, and as shown above the available
1128 NCEP/NCAR dataset had a very poor fit with measured ground temperatures (Table
1129 SM2.3). GSOD data provides air temperature in reasonable agreement with
1130 measured values (Table SM2.4) and a method for estimating hourly ground
1131 temperature values using air temperatures.

1132 Measured ground temperature data for the Isle of May, Ascension Island and Bird
1133 Island were used to derive a relationship between ground temperature, air
1134 temperature, latitude and time of day. Figure SM3.1 shows the average
1135 temperature difference between the air and ground for each hour of the day at the
1136 three field sites (Isle of May (56 °N), Ascension (8 °S) and Bird Island (54 °S))
1137 calculated as the mean of each hour during the measurement period.



1138

1139 **Figure SM3.1 The temperature offset (T_o , °C), difference between average air temperature and ground**
1140 **temperature, for the three field sites during the measurement period (nesting time at each of the**
1141 **colonies): Solid Line: Isle of May (56 °N), Dashed line: Ascension (8 °S) and Dotted Line: Bird Island (54**
1142 **°S).**

1143 Diurnal variation in temperature difference is very similar between the Isle of May
1144 and Bird Island, 56 °N and 54 °S, respectively, where the ground is warmer than
1145 the air throughout the day and night, with a peak during the middle of the day. The
1146 diurnal variation in temperature difference between the air and ground on Ascension
1147 is different, with the ground colder than the air during the night and much hotter
1148 than the air during the day. Although annual variations occur, the focus here is to
1149 provide mean profiles during the bird breeding/nesting seasons.

1150 In the absence of measured global surface temperature data, these were derived
1151 from the air temperature for each colony, using measured surface and air
1152 temperature data from the three field work sites to parameterize a temperature offset

1153 (T_o) function. T_o was set at the measured values: equator = T_o (Ascension), 55 °N
 1154 = T_o (Isle of May) and 55 °S = T_o (Bird Island). Using these fixed points, T_o was
 1155 empirically derived for each hour at any given latitude based on linear interpolation
 1156 between latitudes for these hourly values, hourly T_o values calculated using the
 1157 method presented in Table SM3.1. For sites farther north of the Isle of May and
 1158 farther south of Bird Island values of these sites were used as limits. Due to the
 1159 relatively simple derivation method and the limited number of measurement sites,
 1160 there is substantial uncertainty associated with the estimated surface temperature.
 1161 Further work to improve estimation of T_o compared with T_{air} should be considered
 1162 as part of future work.

1163 **Table SM3.1 Empirically derived temperature offset values T_o for each hour at any given latitude based**
 1164 **on linear interpolation of measured data**
 1165

| Hour of Day | Ground Temperature Offset (T_o , °C) |
|-------------|--|
| 1 | $0.0003 \times \text{Latitude}^2 - 0.8$ |
| 2 | $0.0004 \times \text{Latitude}^2 - 1.0$ |
| 3 | $0.0004 \times \text{Latitude}^2 - 1.2$ |
| 4 | $0.0004 \times \text{Latitude}^2 - 1.4$ |
| 5 | $0.0004 \times \text{Latitude}^2 - 1.5$ |
| 6 | $0.0004 \times \text{Latitude}^2 - 1.3$ |
| 7 | $0.0004 \times \text{Latitude}^2 - 1.0$ |
| 8 | $0.0003 \times \text{Latitude}^2 - 1.1$ |
| 9 | $0.0005 \times \text{Latitude}^2 + 1.8$ |
| 10 | $-0.0003 \times \text{Latitude}^2 + 4.5$ |
| 11 | $-0.0007 \times \text{Latitude}^2 + 7.5$ |
| 12 | $-0.0009 \times \text{Latitude}^2 + 9.0$ |
| 13 | $-0.0009 \times \text{Latitude}^2 + 9.3$ |
| 14 | $-0.0009 \times \text{Latitude}^2 + 9.5$ |
| 15 | $-0.0009 \times \text{Latitude}^2 + 9.5$ |
| 16 | $-0.0006 \times \text{Latitude}^2 + 7.0$ |
| 17 | $-0.0001 \times \text{Latitude}^2 + 3.0$ |
| 18 | $0.0002 \times \text{Latitude}^2 + 0.7$ |
| 19 | $0.0003 \times \text{Latitude}^2 - 0.5$ |
| 20 | $0.0003 \times \text{Latitude}^2 - 0.8$ |
| 21 | $0.0003 \times \text{Latitude}^2 - 0.9$ |
| 22 | $0.0003 \times \text{Latitude}^2 - 0.9$ |
| 23 | $0.0003 \times \text{Latitude}^2 - 0.9$ |
| 24 | $0.0004 \times \text{Latitude}^2 - 1.0$ |

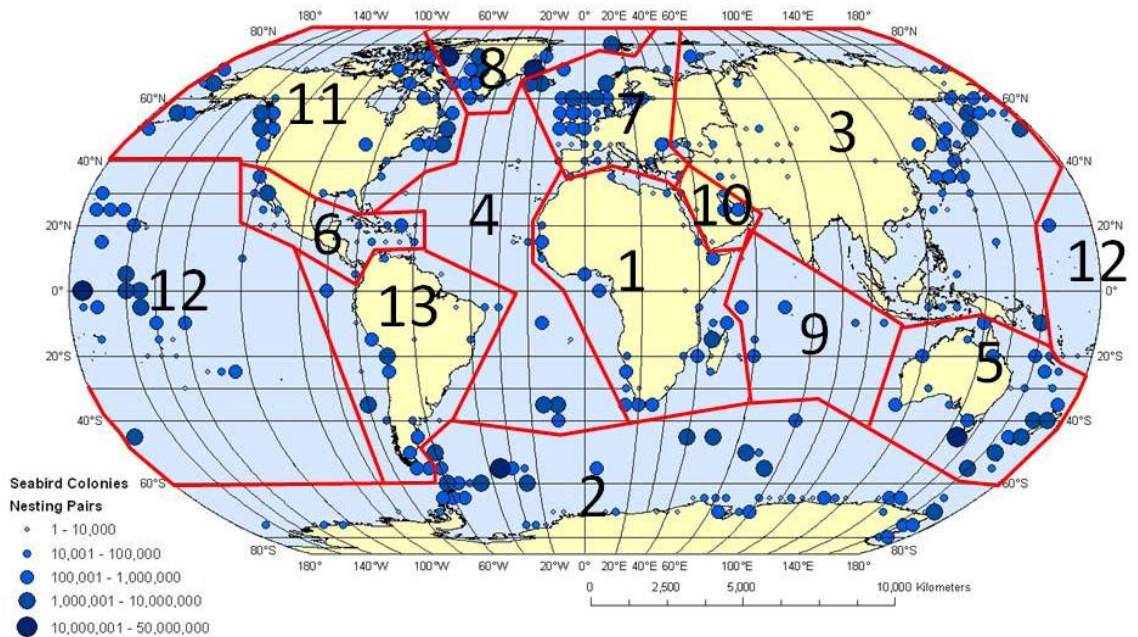
1166
 1167

1168 **Supplementary Material Section 4: A comparison of the NH₃ emission**
 1169 **estimates from the GUANO and TAFE models**

1170 **Table SM4.1 Comparison of the NH₃ emission estimates made by the GUANO model (this study) and the**
 1171 **TAFE model (Riddick et al., 2012 - Scenario 2) and for the ten species with the largest NH₃ emissions, as**
 1172 **calculated by the GUANO model.**

| Species | Model Emission (Gg NH ₃ yr ⁻¹) | | Difference in emission (%) |
|---|---|---|----------------------------|
| | GUANO model | Scenario 2 TAFE model Riddick et al. (2012) | |
| Macaroni penguin | 11.6 | 17.5 | -34 |
| Sooty tern | 10.5 | 4.6 | 128 |
| Guanay cormorant | 8.6 | 4.9 | 76 |
| Chinstrap penguin | 7.0 | 4.2 | 67 |
| Rockhopper penguin | 6.7 | 13.0 | -48 |
| Adelie penguin | 3.3 | 1.8 | 83 |
| King penguin | 2.9 | 10.9 | -73 |
| Laysan albatross | 2.8 | 1.2 | 133 |
| Short-tailed shearwater | 2.2 | 1.2 | 83 |
| Common guillemot | 2.0 | 1.3 | 54 |
| Other penguins | 1.2 | 6.7 | -82 |
| Other species | 11.2 | 15.8 | 29 |
| Total | 81.8 | 83.1 | |
| NH₃ emission penguins | 42% | 65% | |

1173



1174

1175 Figure SM4.1 Global distribution of seabird colonies, based on number of breeding pairs. Lines delineate
 1176 regional boundaries: 1. Africa, 2. Antarctica & Southern Ocean, 3. Asia, 4. Atlantic, 5. Australasia, 6.
 1177 Caribbean & Central America, 7. Europe, 8. Greenland & Svalbard, 9. Indian Ocean, 10. Middle East,
 1178 11. North America, 12. Pacific and 13. South America. To show distribution of the colonies clearly, the
 1179 number of pairs in each 5° grid square have been summed.

1180

1181 Table SM4.2 Regional NH₃ emission estimates calculated by the GUANO model (using modelled ground
 1182 temperature) and the Riddick et al. (2012) thermodynamically dependent bioenergetics (TABE) model,
 1183 Scenario 2.

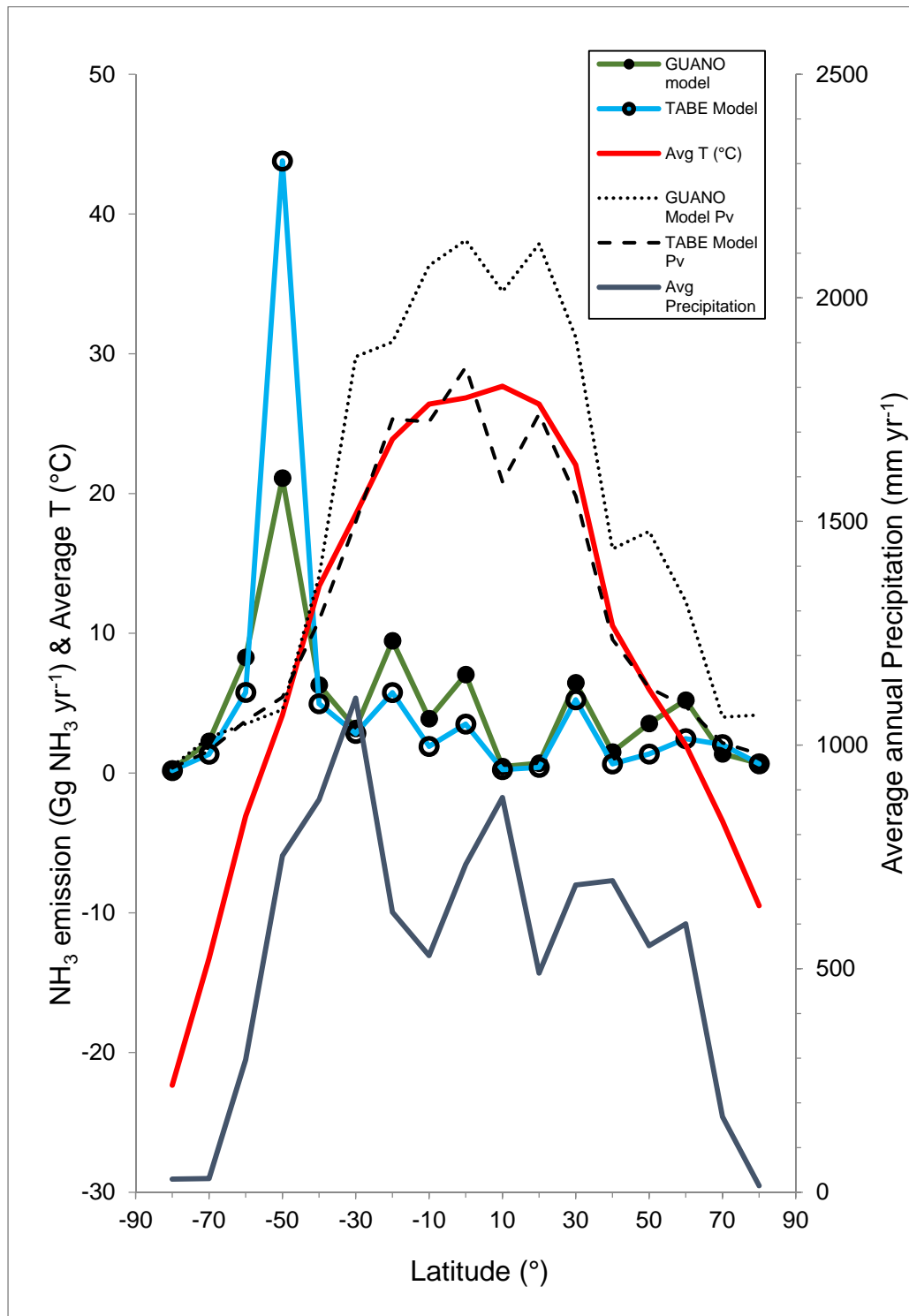
| Region | GUANO Model (Gg NH ₃ Year ⁻¹) | TABE (Scenario 2) (Gg NH ₃ Year ⁻¹) | Difference in estimated emission (%) |
|-----------------------------------|---|--|--|
| 1. Africa | 2.59 | 3.43 | -24 |
| 2. Antarctica & Southern Ocean | 34.2 | 52.7 | -35 |
| 3. Asia | 6.15 | 1.06 | 482 |
| 4. Atlantic | 0.05 | 0.02 | 151 |
| 5. Australasia | 5.46 | 3.18 | 72 |
| 6. Caribbean & Central America | 1.99 | 2.40 | -17 |
| 7. Europe | 1.62 | 2.37 | -32 |
| 8. Greenland & Svalbard | 1.46 | 2.66 | -45 |
| 9. Indian Ocean | 1.14 | 0.53 | 117 |
| 10. Middle East | 1.19 | 1.41 | -16 |
| 11. North America | 3.39 | 1.19 | 186 |
| 12. Pacific | 13.0 | 6.01 | 117 |
| 13. South America | 9.55 | 6.14 | 55 |
| Total | 81.8 | 83.1 | -2 |

1184

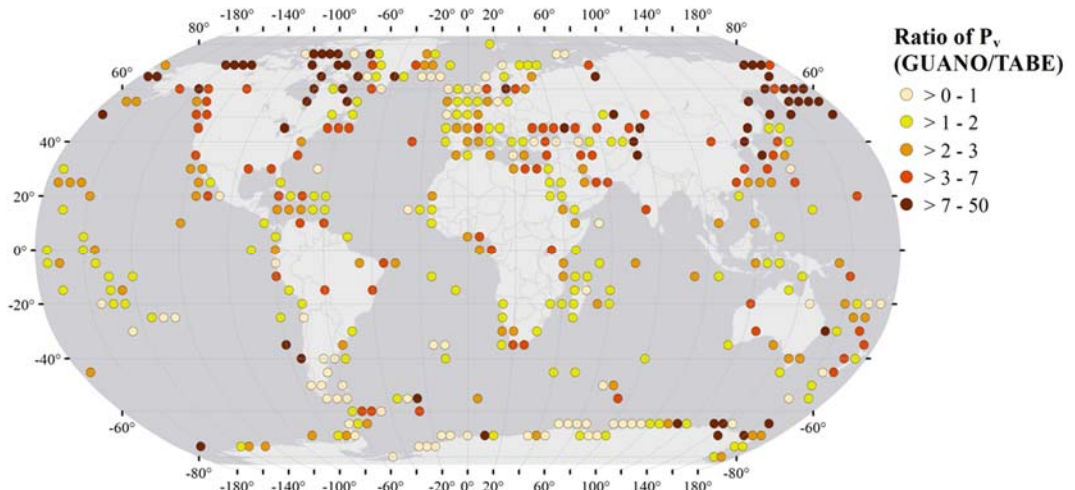
1185

1186

1187 **Supplementary Material Section 5: Relationships between GUANO modelled**
 1188 **NH₃ emissions and environmental variables**
 1189



1190
 1191 **Figure SM5.1 Comparison of the total NH₃ emission estimates made by the Thermodynamically Adjusted**
 1192 **BioEnergetics model (TABE, Riddick et al., 2012 - Scenario 2) and the present application of the GUANO**
 1193 **model (using modelled values for ground temperature). The average ground temperature and**
 1194 **precipitation is also shown and calculated as the average of the hourly values used in the GUANO model**
 1195 **at each colony.**



1196

1197

Figure SM5.2 Global map of the ratio: P_v (GUANO)/ P_v (TUBE)

1198

1199

1200

1201

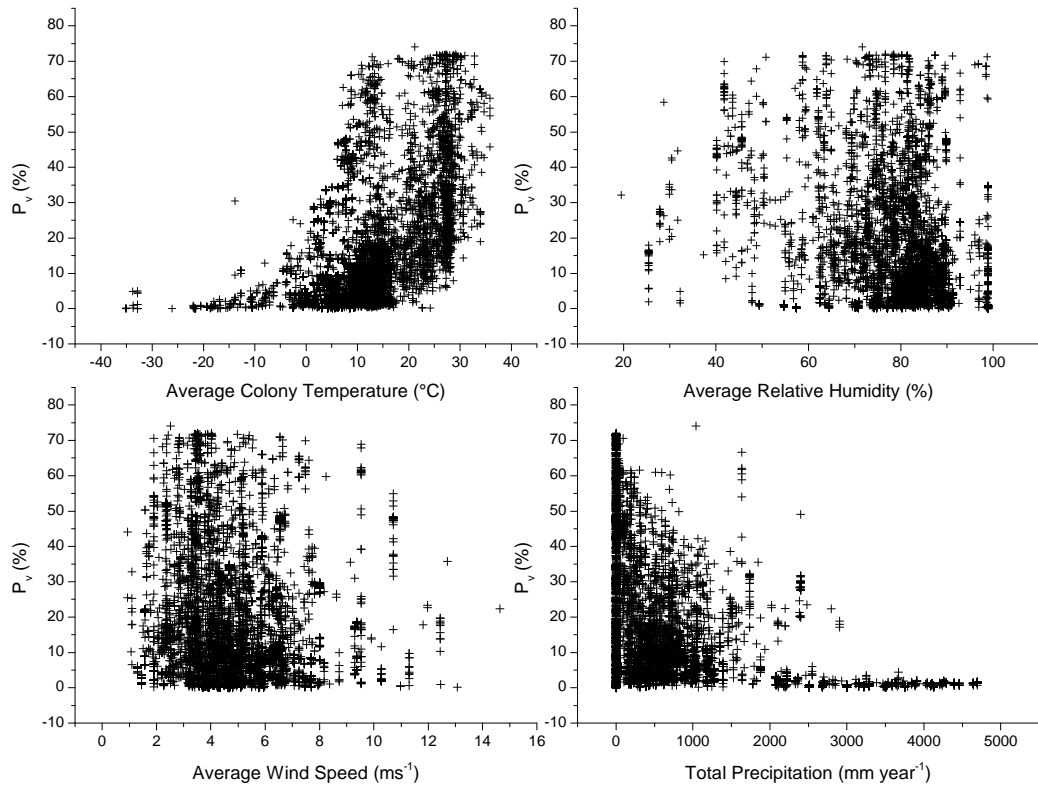
1202

1203

Table SM5.1 The product mean correlation coefficient (r) is calculated for each of the variables used in the GUANO model. RH denotes average relative humidity during the breeding, WS is average wind speed during the breeding season, Total P is the annual total precipitation and $T_{breeding}$ is the average temperature during the breeding season.

| | RH (%) | WS ($m\ s^{-1}$) | P ($mm\ yr^{-1}$) |
|------------------------|----------|----------------------|-----------------------|
| Average $T_{breeding}$ | -0.29 | -0.08 | -0.01 |
| Average RH | | 0.17 | -0.10 |
| Average WS | | | -0.02 |

1204



1205

1206

1207

1208

1209

1210

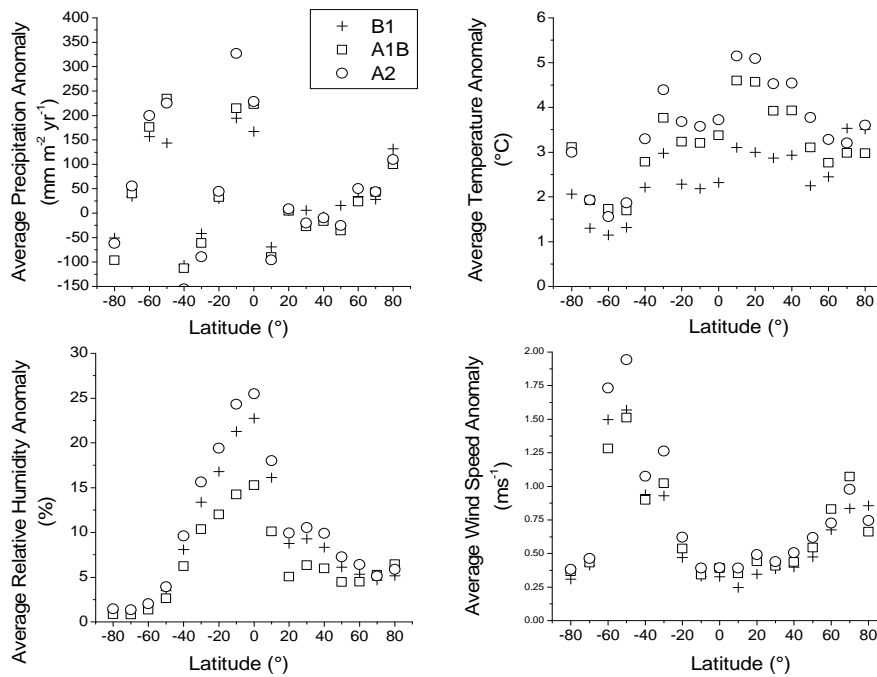
Figure SM5.3 The percentage of nitrogen excreted that volatilizes as NH_3 (P_v , %) plotted, for all colonies in the global seabird database, against the total precipitation (mm year^{-1}), the average wind speed during the breeding season (m s^{-1}), the average relative humidity during the breeding season (%) and the average air temperature during the breeding season ($^{\circ}\text{C}$).

1211 Table SM5.2 Results of a multiple regression analysis of NH₃ emission versus environmental factors in
 1212 the GUANO model. *RH* denotes relative humidity during the breeding season, *WS* is wind speed during
 1213 the breeding season, Total *P* is the annual total precipitation and *T_{breeding}* is the average temperature
 1214 during the breeding season. The range of the variables denotes the variation globally and ΔP_v indicates
 1215 the difference in *P_v* for one unit change in the variable.

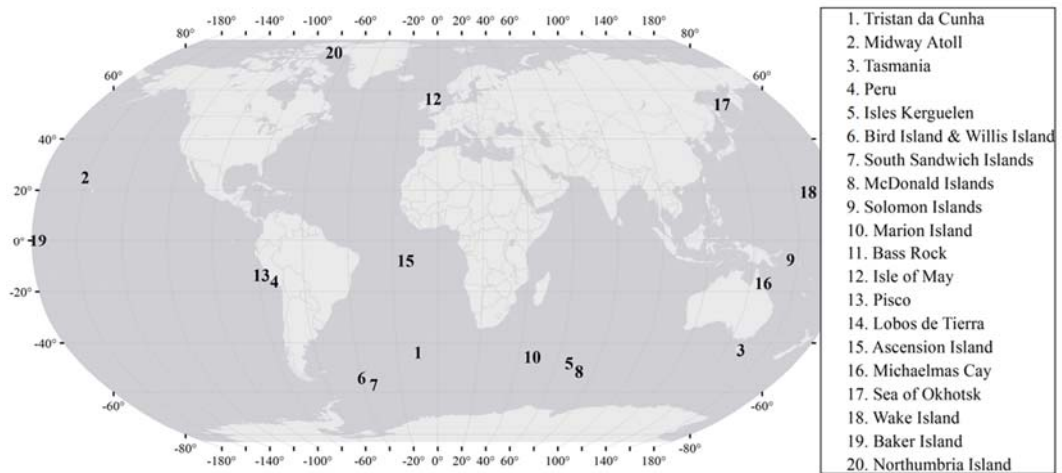
| | Average <i>T_{breeding}</i> (°C) | Average <i>RH</i> (%) | Average <i>WS</i> (m s ⁻¹) | Total <i>P</i> (mm yr ⁻¹) |
|--|--|--------------------------|---|--|
| Maximum | 36 | 100 | 11 | 4700 |
| Minimum | -35 | 40 | 1 | 0 |
| Average | 11 | 89 | 5 | 845 |
| ΔP_v per 1 unit of variable (%) | 0.97 | 0.10 | 0.22 | -0.006 |
| p-value | $< 2 \times 10^{-16}$ | 2.2×10^{-13} | 0.003 | $< 2 \times 10^{-16}$ |

1216

1217 **Supplementary Material Section 6: Guano modelled NH₃ emission response**
 1218 **to a changing climate**
 1219



1220
 1221 **Figure SM6.1 Climate change anomalies for IPCC climate change scenarios B1, A1B and A2 for**
 1222 **precipitation, temperature, relative humidity and wind speed.**



1223
 1224 **Figure SM6.2 Map of notable seabird colonies discussed in paper**

1225
 1226 **Table SM6.1 Climate change anomalies of IPCC scenario A2 and the predicted change in P_v at the largest**
 1227 **seabird colonies. ΔP_v indicates the change in P_v between the 2010 estimates and the predicted values for**
 1228 **2099**

| Colony | Latitude | A2 Precip Anomaly (mm yr ⁻¹) | A2 Temp Anomaly (°) | A2 Wind Speed Anomaly (ms ⁻¹) | A2 Relative Humidity Anomaly (%) | ΔP _v 2010 to 2099 (A2) (%) |
|------------------|----------|--|---------------------|---|----------------------------------|---------------------------------------|
| Tristan da Cunha | -37 | -122.2 | 3.8 | 1.9 | 11.4 | 32.5 |
| Midway Atoll | 28 | 1.3 | 5.5 | 0.4 | 6.8 | 26.1 |

| | | | | | | |
|--------------------|-----|-------|-----|-----|------|------|
| Tasmania | -44 | -93.5 | 2.1 | 1.5 | 5.1 | 11.2 |
| North Coast Peru | -20 | -39.8 | 4.1 | 0.2 | 19.7 | 3.9 |
| Isles Kerguelen | -49 | 247.4 | 1.5 | 2.2 | 3.0 | 0.4 |
| Willis Island | -54 | 278.8 | 1.4 | 2.4 | 2.5 | 0.2 |
| South Sandwich Is. | -58 | 258.3 | 1.4 | 2.4 | 2.3 | -1.7 |
| McDonald Islands | -53 | 282.7 | 1.2 | 2.8 | 2.3 | -6.5 |

1229

1230

1231 Table SM6.2 Regional NH₃ emissions (Table A) and P_v (Table B) estimates for GUANO model 2010 and
 1232 2099 using all data and individual meteorological anomalies
 1233 Part A

| Region | EMISSIONS (Gg yr-1) | | Future scenarios for 2099 | | | |
|--------------------------------|---------------------|--------------------------------------|------------------------------------|--------------------------------------|--------------------------------------|--|
| | 2010 | With 2099 wind anomaly only | With 2099 RH anomaly only | With 2099 PPTN anomaly only | With 2099 Temp anomaly only | 2099 with all 4 climate anomalies included. |
| Africa | 2.59 | 2.61 | 3.99 | 2.85 | 3.62 | 4.78 |
| Antarctica & Southern Ocean | 34.20 | 35.43 | 40.32 | 22.80 | 42.97 | 35.08 |
| Asia | 6.15 | 6.19 | 7.59 | 4.67 | 9.26 | 8.91 |
| Atlantic | 0.05 | 0.05 | 0.06 | 0.03 | 0.06 | 0.07 |
| Australasia | 5.46 | 5.57 | 8.25 | 6.53 | 7.25 | 12.52 |
| Caribbean & Central America | 1.99 | 1.99 | 2.33 | 1.99 | 2.70 | 2.89 |
| Europe | 1.62 | 1.64 | 2.45 | 1.68 | 2.57 | 3.77 |
| Greenland & Svalbard | 1.46 | 1.47 | 2.18 | 1.28 | 2.50 | 3.38 |
| Indian Ocean | 1.14 | 1.16 | 1.78 | 0.94 | 1.42 | 1.94 |
| Middle East | 1.19 | 1.19 | 1.43 | 1.23 | 1.42 | 1.52 |
| North America | 3.39 | 3.45 | 4.36 | 6.06 | 5.15 | 6.62 |
| Pacific | 13.04 | 13.11 | 18.48 | 9.53 | 17.38 | 19.70 |
| South America | 9.55 | 9.57 | 11.63 | 10.79 | 10.77 | 12.62 |
| Grand Total | 81.83 | 83.43 | 104.87 | 70.38 | 107.07 | 113.79 |

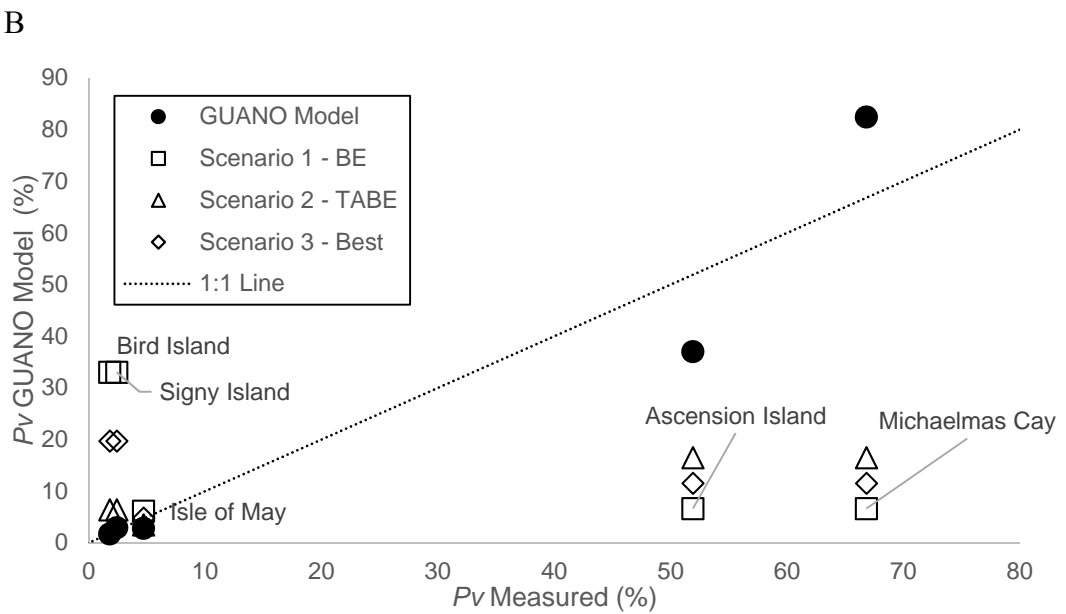
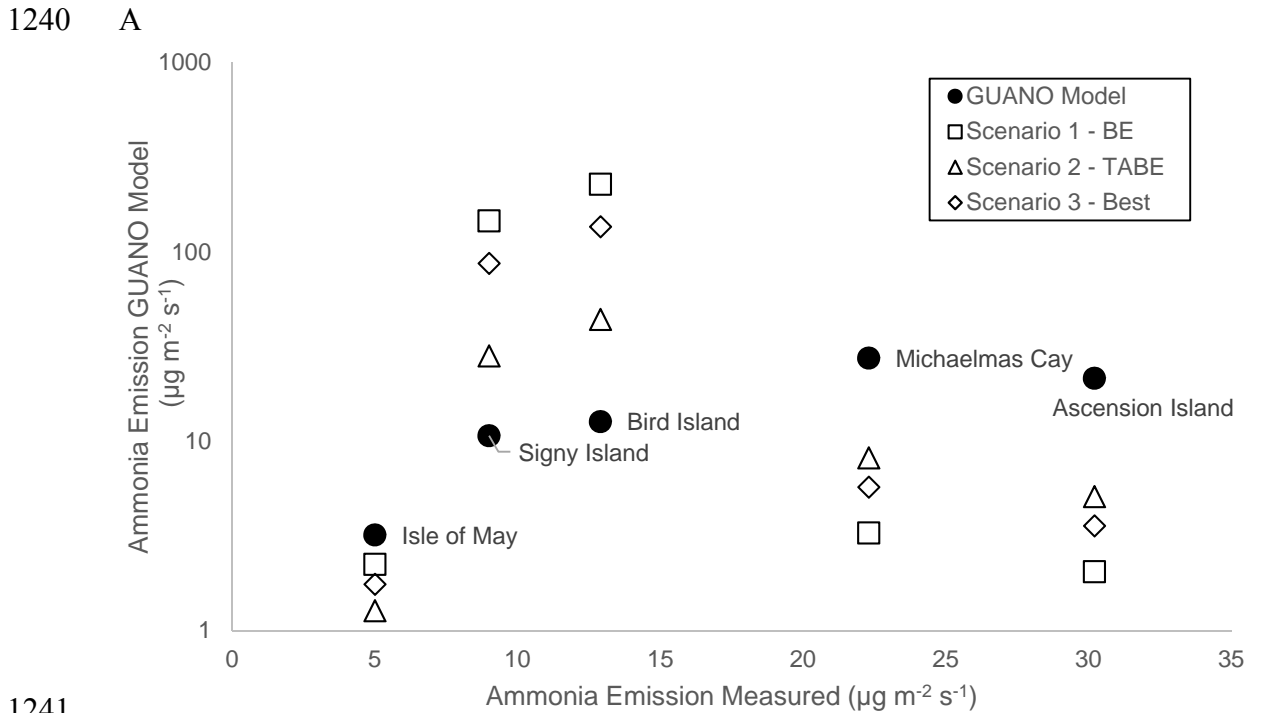
1234

1235

1236

1237

| Region | P_v (%) | | Future scenarios for 2099 | | | |
|-----------------------------|-----------|-----------------------------|---------------------------|-----------------------------|-----------------------------|---|
| | 2010 | With 2099 wind anomaly only | With 2099 RH anomaly only | With 2099 PPTN anomaly only | With 2099 Temp anomaly only | 2099 with all climate anomalies included. |
| Africa | 28.1 | 28.6 | 40.2 | 30.1 | 38.8 | 47.7 |
| Antarctica & Southern Ocean | 4.0 | 4.1 | 5.0 | 3.2 | 5.2 | 5.3 |
| Asia | 15.8 | 15.9 | 21.8 | 14.2 | 24.9 | 28.9 |
| Atlantic | 40.4 | 41.1 | 57.9 | 31.6 | 56.7 | 68.6 |
| Australasia | 23.1 | 23.6 | 32.4 | 28.7 | 29.2 | 42.0 |
| Caribbean & Central America | 36.9 | 37.0 | 47.2 | 37.5 | 48.0 | 56.0 |
| Europe | 11.0 | 11.1 | 17.5 | 12.2 | 17.8 | 26.9 |
| Greenland & Svalbard | 4.1 | 4.2 | 5.4 | 3.4 | 6.2 | 7.1 |
| Indian Ocean | 29.8 | 30.2 | 47.5 | 24.1 | 38.4 | 53.6 |
| Middle East | 43.9 | 44.1 | 56.0 | 45.8 | 56.1 | 62.9 |
| North America | 19.8 | 19.9 | 23.6 | 24.7 | 27.9 | 34.1 |
| Pacific | 34.6 | 34.9 | 48.9 | 27.2 | 46.0 | 53.7 |
| South America | 27.2 | 27.5 | 30.5 | 24.0 | 30.3 | 33.4 |
| Global Average | 6.2 | 8.6 | 8.1 | 6.3 | 5.3 | 7.9 |



1243

1244 **Figure SM6.3. Comparison of (A) the area-based NH₃ emission value and (B) the *P_v* value**

1245 **calculated by the GUANO model with micrometeorological measured data for site based**

1246 **measurements. Values refer to the periods of the measurements used. For further details see**

1247 **Riddick et al. (2014; 2016a; 2017). Sites: Sooty terns on rocks, Ascension Island (Mid Atlantic);**

1248 **Puffin burrow area with grass, Isle of May (Scotland); Macaroni penguins on rock, Bird Island**

1249 **(South Georgia, South Atlantic); Common noddys on bare ground, Michaelmas Cay**

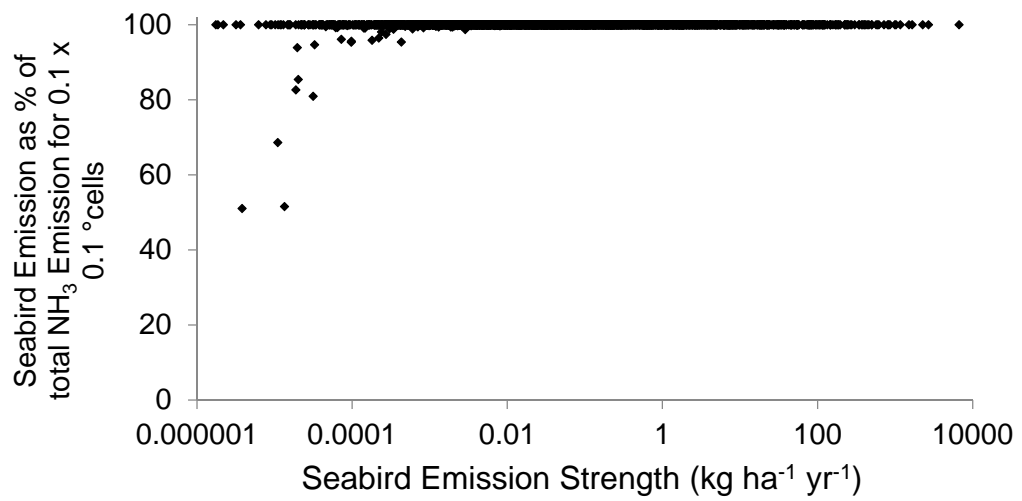
1250 **(Northern Australia); Chinstrap penguins on bare rock, Signy Island (South Atlantic). Also**

1251 **presented are matching estimates calculated by Riddick et al. (2012): Scenario 1: BE Model,**

1252 **Scenario 2: TABE model and Scenario 3: The best estimate of.**

1253

1254 **Supplementary Material Section 7: Contribution of seabird NH₃ emissions as**
1255 **estimated here as a percentage of total NH₃ emissions from seabirds and**
1256 **other sources**



1257

1258 **Figure SM7.1 Contribution of seabird NH₃ emissions as estimated here as a percentage of total NH₃**
1259 **emissions from seabirds and other sources (estimated by the EDGAR database (version 4.1) of EC-JRC,**
1260 **2010). The figure includes 9,549 dots, where each dot represents a 0.1 by 0.1 degrees square containing**
1261 **at least one modelled seabird colony.**